QATAR UNIVERSITY

COLLEGE OF ENGINEERING

NUMERICAL ANALYSIS OF A SACRIFICIAL CLADDING PANEL SUBJECTED TO LOCALIZED NEAR-FIELD IMPULSIVE LOAD

BY

NOUMAN NABEEL MOH'D. N. ALQWASMI

A Thesis Submitted to

the Faculty of the College of Engineering

in Partial Fulfillment of the Requirements for the Degree of

Masters of Science in Mechanical Engineering

June 2019

COMMITTEE PAGE

The members of the Committee approve the Thesis of

Nouman Nabeel Moh'd. N. defended on 17/04/2019.

Professor Faris Tarlochan

Thesis/Dissertation Supervisor

Dr. Sadok Sassi

Committee Member

Professor Khaled Abou-El-Hossein

Committee Member

Approved:

Abdel Magid Hamouda, Dean, College of Engineering

ABSTRACT

ALQWASMI, NOUMAN, NABEEL MOH'D. N., Masters: June : 2019, Masters of Science in Mechanical Engineering

Title: Numerical Analysis of a Sacrificial Cladding Panel Subjected to Localized Near-Field Impulsive Load

Supervisor of Thesis: Faris Tarlochan.

Extensive research focus had been given to sacrificial sandwiched panels used to mitigate the effects of blast loads. This is due to their ability to distribute the load and absorbing significant portions of the blast energy. This numerical research studies the behavior of sacrificial sandwiched panels with axially oriented octagonal tapered core tubes subjected to near-field impulsive blast loading. The deformation behavior and a number of assessment parameters consisting of the peak force, stroke efficiency, energy absorption, and core efficiency were analyzed. The developed deformations modes were mainly influenced by the top plate and tube thickness. Tubes of a 5° taper performed unfavorably, exhibiting increased peak force and lower energy absorption. Moreover, panels of top plate thickness of 4 mm exhibited higher stroke efficiency as compared to panels of lower thickness. Furthermore, the top plate and tube thickness recorded the highest influence on energy absorption. Finally, a percentage increase of 73.5% in core efficiency was observed for thick-plated panels as compared to thin-plated ones.

DEDICATION

I dedicate this thesis to the community I am living in of Muslims and Arabs, to my family and friends.

ACKNOWLEDGMENTS

I truly am very grateful to my invaluable parents, my mother, Manal, and my father, Nabeel, raising a firmly-bonded family and supporting their children all the way to the top. To my siblings, Doa'a, Sara, Abdullah, and Jana who enhanced the quality of my life, motivating my progress, and being optimistic about my future. To my supervisor, prof. Faris, leading me in this thesis till the end, and being patient and considerate with every step.

This project was carried out in the Mechanical and Industrial Engineering Department of Qatar University. I need to thank all the faculty members who supported this project with their great ideas, and the help provided by them at hard times.

TABLE OF CONTENTS

LIST OF TABLES

LIST OF FIGURES

CHAPTER 1. INTRODUCTION

1.1. Problem Statement

Threats from terrorist attacks is increasing day-by-day due to the greed of terrorists to accomplish their wrongly routed goals. One of the most famous terror attacks was the 11th September 2001, and recently terrorists are launching attacks in Europe and the Middle East. For a big harm coverage area, terrorists rely on bombings which cause loss of personnel, governmental and public properties whenever the explosion is in the vicinity. Impulsive loading from an accidental chemical plants' explosion or an intended explosive detonation create shock waves of several Mach [1].

Safety of innocent people is of the highest priority in the event of bombings in wars and terrorist attacks, and even chemical plant's accidental explosions. A bomb detonation is associated with the sudden expansion of the medium surrounding the bombs' structure, which causes a shock wave to propagate radially outward of the bomb's center. The shock wave and flying debris resulting from the detonation heavily contribute to the damage accompanying the loading event. Safety from blast loading is related to the applications of structural engineers, where their goal is to alleviate the loading on the protected structures, that are adjacent to the impulse load. The U.S.A. department of defense (DoD) defined a five-level protection criterion (Table 1) that acts toward Anti-terrorism (AT) standards.

Table 1. DoD Anti-Terrorism Level of Protection Standard [2]

Level of protection	**Potential structural damage**	**Potential injury**
Below AT standards	Massive destruction	Major fatalities
Very low	Onset of structural collapse	Major serious injuries and a fatality percentage range of 10 – 25%
Low	Unrepairable damage	Major significant injuries and fatality percentage of <10%
Medium	Repairable damage	Minor injuries and fatalities are unlikely
High	Superficial damage	Superficial injuries

It is evident from the precious table that the fatalities' threat from explosions could reach up to very high levels. Therefore, research proceeded with finding a solution to the bombing detonation problem. Energy absorbing devices were of the highest potential to act as a solution to this problem, as their role is to control the absorbed amount of impact energy, to reduce the impact intensity either on non-sacrificial structures or occupants of a vehicle. The concept of blat resistant walls and structures dates to the second world war, where bomb shelters protected against explosions. Further assessments were given to water walls, steel mesh filled with soil, pre-cast concrete, and even steel-concrete-steel sandwich panels [2]. Moreover, monolithic plates made up of metals or composites acted as good energy absorbers in these scenarios, with thickness being the determining factor to an optimized plate

performance [3]. With all these structures accounted for, sandwich panels were found to be the current trending solution for an excellent energy absorber in blast scenarios [4]. This is due to their ability to distribute the load prior to absorbing significant portions of the blast energy. Sandwich panels consisted of three essential components, a load distributor top-plate, an energy absorbing core, and an intact back-plate. Sacrificial cladding structures are usually implemented on building walls [5], and can also be implemented on vehicles or ship hulls, subjected to landmines and underwater explosions, respectively [6,7].

Structures referred to as "Crashworthy" devices intend to reduce the damage on structures impacted dynamically, to save the lives of occupants inside [8]. The concept of crashworthy devices is very common in the field of saving automotive bodies from crash scenarios, and thin-walled structures received most of the focus in this field. The reason behind this care revolves around the great energy absorption, ease of manufacturing and installation, and lightweight characteristics that thin-walled structures possess. Furthermore, thin-walled structures are the component filling the core of a sacrificial cladding panel.

1.2. Armored structures

One way to prevent IEDs (i.e. improvised explosive devices) and landmines threat is by demining, but these are very expensive, dangerous and time consuming. The other solution is to design and engineer structures that can withstand blast effects, known as armored structures [9]. A lot of effort had been directed toward the use of monolithic plates in thoroughly securing the perimeter of an occupant carrying MRAP (i.e. mine resistant ambush protected) vehicles or the walls of an occupied building. Moreover, recent research had shed light on the performance of sandwich and sacrificial

panels under the same blast loading conditions. Where these panels were claimed to have better blast resistance capabilities over monolithic plates in small-scaled loadings [10]. This favor is mostly due to the more complex three-essential components of a Sandwich panels and sacrificial claddings, composed of a load distributor top-plate, an energy absorbing core, and a further deforming or an intact back-plate [11]**.**

The mode of deformation and panel performance are affected with the different material, dimensions employed and the geometry of the components in the panel. Although the plates of the sacrificial panels were extensively researched for a better performance, but they were considered as the secondary concern after the energy absorbing core. The former match the description of an individual blast energy mitigating plate; studying them for monolithic and composite materials [12–15], to overcome the problem of weight that goes hand-in-hand with the ease maneuverability of vehicles, and, structural manufacturing and implementation expenses.

Furthermore, thinking of the core as a separate component received much more focus than the full assembly of the panels. Core structure's behavior differs with varying the material, geometry, and the loading type. Minor research had focused on the addition of multi-layers of ductile metal plates to act as a sandwich structure, mainly, different grades of steel and aluminum. Recent research had focused on the addition of cellular material (i.e. foams) to the core, considering composites, such as fiber-reinforced composites, consisting of metal foams with uniform [16,17] and non-uniform [18,19] density distribution. To fully understand the differences in behavior between metals and composites, it is mandatory to mention the plastic energy dissipation mechanism of these materials. The ductile metallic structures dissipate energy by creating progressive or out-off plane folds under plastic crushing [20]. While composite ones dissipate energy by undergoing brittle failure with composite layers

delamination, matrix cracking, and fibers breakage [21].

Aside from the concept of sandwiching lump structures, thin-walled structures were another engineering design that undergoes crushing upon impact with an external force. Thin-walled structures registered distinct and excellent performance in the aspect of energy absorption in impact events, absorbing energy by permanent compression failure, acting as a sacrificial structure [22]. Research directed some attention to integrating the concept of thin-walled structures and foams, to obtain an enhanced energy absorbing performance in a more controlled manner [23–26]. Equally important, two possible orientations were considered for thin-walled structures in panels' core: axial and lateral placements. The former placement is more prone to Euler mode (i.e. off-axis) of buckling than the latter which significantly reduces the energy absorbing capacity of the crushed tube. Despite higher instability, hence, lower energy absorption is associated with axially loaded members, but, if crushed progressively, they were found to absorb ten folds of energy compared to laterally loaded structures [27]. Corrugated, square and circular laterally oriented tubes, were studied by several researchers to assess their performance against blast loading [28,29].

Axially loaded thin-walled structures in all types of loading (i.e. quasi-static, dynamic and impulsive loading) are similar in configuration, but their application field is different. Due to this similarity, a general over-review under all loading types of the research concept on thin-walled structures is to be done. Regarding geometrical variations, the most studied cross-sections are the square and circular, displayed for all types of loading. Also, inconvenient cross-sections were examined to further assess the performance, ranging from polygonal cross-sections, star-shaped, and even cellular structure with defined patterns, such as the honeycomb pattern. Multi-cells and bi-tubular members were an addition to axially crushed structures, regulating crush

progression [30]. Moreover, an investigation on the introduction of triggers along the surface of the energy absorbing structures was carried, they worked on enhancing the energy absorbing ability and lowering the crushing forces on the protected structures [31]. Surface patterns had one of the most positive effects on controlling the crushing behavior in the structures, where corrugated, tapered and origami patterns all played a significant role enhancing the performance [32,33].

In the event of close-range and contacting explosives, sacrificial panels are subjected to more severe load schemes. Near-field detonated explosives tend to cause the forces on the top plate, hence the whole structure, to be localized in a specific region (i.e. non-uniformly distributed across the top plate). Localized forces on the structure causes the top plate to be easily breached, and if not, exposes the core to severe oblique loads [34]. Researchers always intend to make structure deform axially, while in contrast, oblique loads cause the energy absorbing structures to deform in an Euler mode, significantly reducing the overall energy absorbed. Therefore, researchers had to direct their interest to overcome the problem of oblique loads. Thin-walled tubes with small aspect ratios, conical and tapered surface patterns were the main research focus in this field. The care shifted to these structures because of their ability to outturn failing by global euler buckling that results from oblique loads. Reid and Reddy [35] deduced that tapered tubes are preferred to straight ones under oblique loading, as they are less vulnerable to fail in the off-axis buckling mode. Since then, tapered tubes were further researched in many aspects to extend their ability of absorbing energy in a more controlled manner. Once again, all aforementioned structural modifications were considered in tapered tubes; studying the performance of empty and foam-filled [36–43], different cross-sections [44], the introduction of triggers [45,46], unconventional surface patterns [33,47], and multi-cellular configurations. Majorly, it was deduced that

tapered tubes performed superior to straight tubes under oblique impacts.

From the preceding discussion, it is evident that the full understanding of the performance of sacrificial panels with axial thin-walled structures to localized blast loading is lacking. It is also apparent that octagonal tubes offer higher energy absorption capacity than tubes of other geometrical cross-sections. Furthermore, tubes of tapered profiles have proven advantageous under oblique loadings as compared to the conventional straight tubes. Due to the difficulties met to run blasted structures experiments, finite element methods will be the analysis method for this thesis. Therefore, the aim of this thesis is to numerically design a sacrificial cladding panel of octagonal tapered tubes (i.e. OTT's) as core for the full assessment of the energy absorbing and load mitigations characteristics under near-field impulsive loading. The numerical analysis was carried out using the finite element code Abaqus/Explicit. Different geometrical configurations of panels, namely the tube taper angle, tube aspect ratio, tube and top-plate thicknesses, the ratio of width-to-length of the cross-section were proposed to study their influence on the panel's behavior.

1.3. Thesis aim, objectives and methodology

1.3.1. Aims and objective

This thesis aims to design and assess the performance of sacrificial cladding panels with conventional top and bottom plates, and thin-walled octagonal tapered core tubes subjected to near-field impulsive load to mitigate blast loadings on protected structures. This aim is accomplished through the following objectives:

1. Develop a finite element model to simulate the propagation of the stress wave and the deformation of the top plate and the core tubes under localized impulsive load, then, calibrate it with published experimental data.
2. Carrying a parametric study on the effect of tube taper angle, tube aspect ratio, tube and top-plate thicknesses, the ratio of width-to-length of the cross-section on the response of the blast loaded panel.
3. Comparing the energy absorption and peak load response of the proposed panels with previously published work from literature to gain an insight of how enhancements where implied in the current designs.

1.3.2. Methodology

Non-linear finite element analysis was used to simulate the performance of the sacrificial panels with newly designed core tubes, that are subjected to a localized blast load numerically. The core is composed of axially oriented octagonal straight (OS) and tapered (OT) tubes with a specific clearance between each tube and the adjacent one, to avoid contacting during buckling. Finite element analysis is one of the most efficient measures in reducing the financial and time cost of research. The explicit solution code of Abaqus package was used to model, solve and visualize the simulations available for study. All the components are made of mild steel, where the inertial characteristics were obtained from a previously published research work, and the strain-rate hardening effects where employed from the Cowper-Symonds relation for the assignment of the dynamic buckling behavior of the material. For the full assessment of the OS and OT tubes, different geometrical parameters of the taper angle, aspect ratio, tube thickness and cross-section's ratios were used. To gain an insight of the effect of the panel configuration on the performance on the tubes, the top-plate thickness was also varied.

1.4. Contributions

Thin-walled structures as cores in sacrificial panels recorded promising energy absorption and controllability measures in the field of impulsive loading. Adding to the fact that near-field loading contributes to initialize oblique loading on panels, due to the localized region of impact. Tapered thin-walled tubes impacted in axial directions performed similar to straight tubes, but, superior under oblique impacts. Octagonal cross-sections of tubes, although unconventional, recorded higher energy absorption per crushed length characteristics than conventional square and circular tubes, prior to the condensations of the buckled folds in the tubes. Therefore, this thesis covers newly designed thin-walled tubes with a taper profile along the length and an octagonal cross-section across the core tubes of the sacrificial panels. The assessed characteristics of interest are the energy absorption of the core structure, and, the transferred loads to the non-sacrificial structure that the panel is attached to.

1.5. Thesis Layout

Shown in this sub-section the organization of the thesis, reaching up to the conclusion, as follows:

CHAPTER 1. INTRODUCTION

In this chapter, firstly, an introductory of what issue lead to this topic given as a problem statement, the current solutions present to it, and the proposed research topic of this thesis. So forth, working on the aims and objectives, reaching up to the contributions served by this work, to the field it is revolved around.

CHAPTER 2. LITERATURE REVIEW

While this thesis works on shock loading, this chapter surveys the physics of blasts in air, flowing to the loading performance of sacrificial structures against the

different strain-rates, i.e. of quasi-static, dynamic and impulsive loading. Finalizing a summary statement reasoning the studied work held in this thesis of sacrificial panels with tapered octagonal core tubes, relating it to the surveyed literature.

CHAPTER 3. METHODOLOGY

This chapter focused on the functionality of the numerical tool used for analysis. Firstly, describing the finite element package used for analysis. Followed by a full description of the geometrical, material and the boundary conditions' models. Depending on this algorithm, finally, a validation scheme is set to assure the viability of the model in analyzing the response of the system.

CHAPTER 4. SACRIFICIAL CLADDING PANEL SUBJECTED TO NEAR-FIELD

This chapter fully builds up on the previous one, carrying the analysis on the sacrificial panels with octagonal tapered tubes as core. The analysis deals with assessing the performance of the panels of interest for the buckling behavior of the crushed core tubes, and so forth, it's relevance to the energy absorbing capability of the panel. For this to comply, certain assessment performance parameters were of use, focusing on the reaction force of the non-sacrificial structure, stroke efficiency of the tubes, and the energy absorption capability of the system.

CHAPTER 5. CONCLUSIONS

An inclusion of a brief description of the thesis research proposal, and, restating a summary of the final findings acquired from running a study of the proposed system.

CHAPTER 6. RECOMMNEDATIONS FOR FUTURE WORK

This chapter sheds light on a recommended future research work for a further understanding and a possible enhancement of a similar or an alternative system, to act as a better solution for the introduced problem.

CHAPTER 2. LITERATURE REVIEW

2.1. Introduction

This chapter will offer a review on the previous findings related to this thesis's field, up to this date. Literature review is responsible for displaying a clear image of the different aspects undertaken of theories, models, and findings to shine the light on the path crossed to reach this thesis idea. The sequence and topics of the sub-sections covered in this chapter are the following:

(1) Blast loading

(2) Structural crashworthiness and impact

(3) Structural basis for energy absorption

(4) Sacrificial cladding structures

(5) Finite element analysis (FEA)

2.2. Blast loading

The occurrence of a shock wave could be a result of a terrorist attack, war bombings, war mines leftovers and chemical laboratory explosions. Thereafter, blast loads being catastrophic events, could be used for destructing a wide variety of structures, including ship hulls, aircrafts, automobiles, and civil structures. Prior to facing the threat held from shock waves produced from blast sources and mitigating it, a full understanding of the mechanism of a propagating shock wave, exclusive to air medium, must be presented first.

2.2.1. The physics of blast loading

Shock waves are produced from within the three classifications of explosions, that is, physical, nuclear or chemical explosions [48]. Physical explosions arise from no chemical reaction taking place, rather, a meaningful example would be the explosion of a highly compressed gaseous cylinder, and can also include natural phenomena, such as the eruption of a volcano. On the other hand, nuclear explosions arise from the activities happening at the subatomic level of elements, and when splitting of these elements' particle is to happen an enormous amount of energy would be released upon detonation. Finally, for the contest of this thesis, chemical explosion is the type of explosion to be exclusively discussed in this section of the thesis. Chemical explosions arise from the rapid oxidation of the key components of explosives, which are carbon and hydrogen, resulting in the production of highly compressed gas, and the release of approximately 4389 kJ/kg equivalent of TNT (i.e. Trinitrotoluene compound) [48]. The medium which the post-explosion products is to propagate in highly affects the characteristics of the shock; shock pressure is referred to the explosion products that propagate in a solid, and a shock wave when a fluid medium is the case. Air blasts and underwater blasts lie under the fluid medium case, with the review pinning points solely on the former one.

Chemical explosions further split into two product releasing mechanisms, namely, deflagration and detonation. The defining criteria is the burning rate of the explosion components; if the burning rate is slower than the speed of sound in the same components, then the process is called deflagration, otherwise it is detonation [48]. Deflagration processes are carried out by propellants, while, detonation processes are carried by high explosives, where recent products of these explosives depend on the nitrate-based compounds, as the previous mentioned product of TNT [49]. Since a brief

introduction on the physical properties of an explosive was given, it is time to shift the focus to the class of interest, which is chemical detonations.

Whenever an explosive is detonated in air, a sudden shock front (thin boundary) leads the propagating gas, because of the pressure difference between the pressurized gas and the medium [50]. Once the shock front reaches the structure at the arrival time (t_a), an impulse peak pressure (P_0^+) is created. Following P_0^+ are two phases: the positive and the negative phases of the explosion (Figure 1). The positive phase is ahead with an approximated exponential decrease from the peak pressure, with a phase duration of t_0^+, which makes this phase an essential component in blast applications. The negative phase is next, with the ambient pressure at a specific point in the structure being below atmospheric pressure, reaching a minimum of P_0^-, and having a duration of t_0^-. Despite the negative phase being noticeable and longer in duration, but, the negative phase's amplitude is insignificant in comparison to the positive phase, hence is ignored. Regarding transverse blasted flat components, Figure 2 depicts the image of an ideal spatial pressure profile acting on the face of a blast loaded plate.

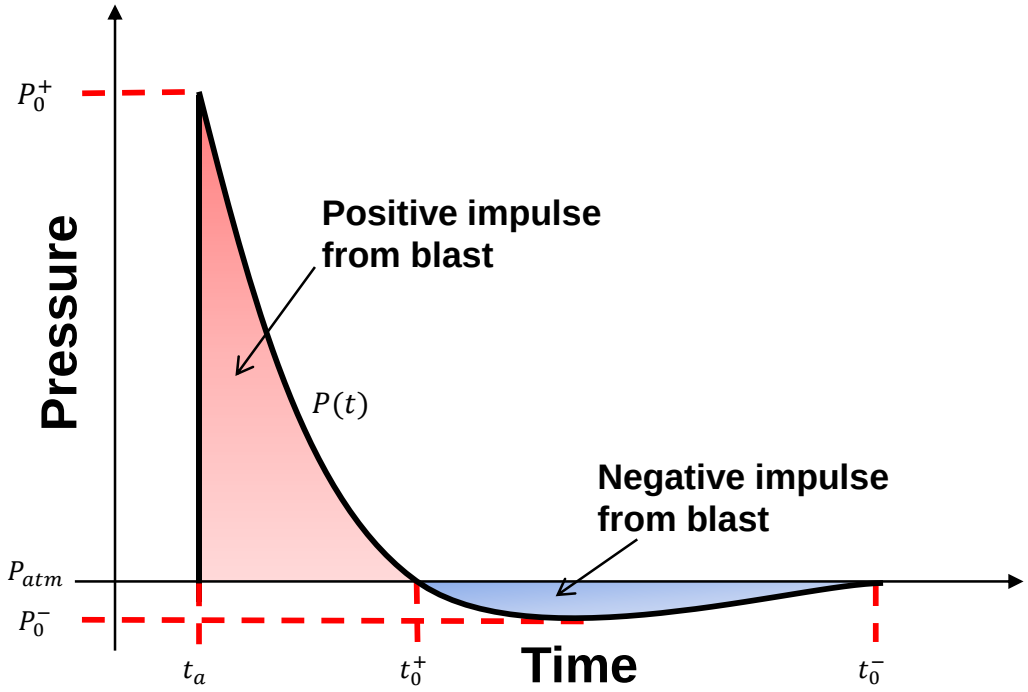

Figure 1. Ideal pressure-time profile of a blast event at a specific stand-off

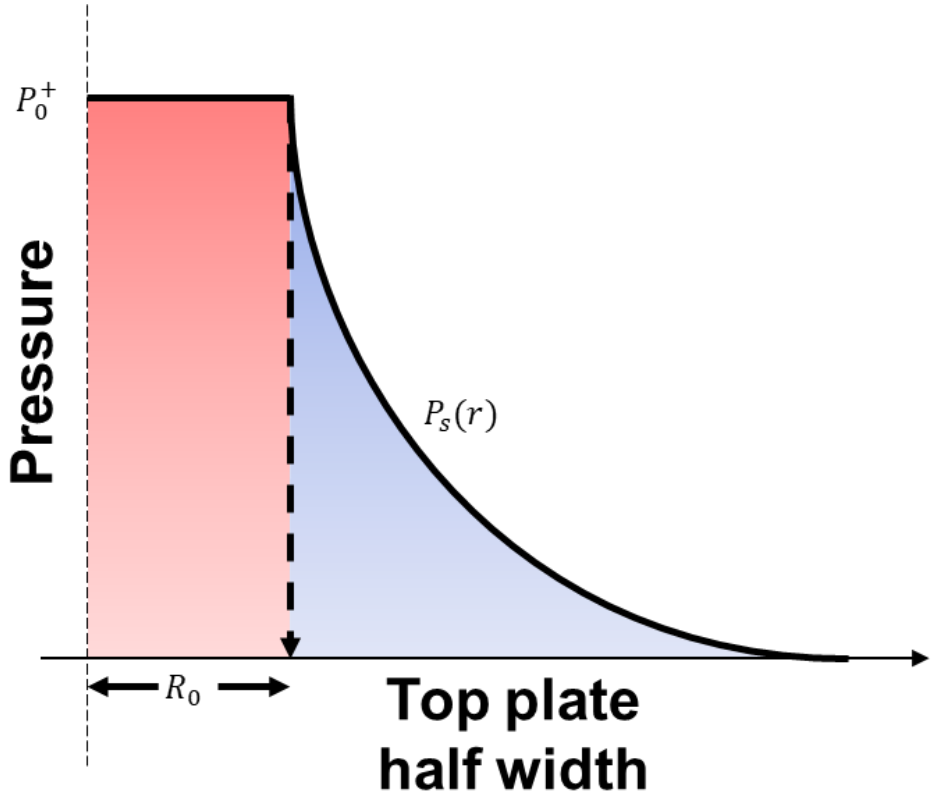

Figure 2. Ideal pressure-space profile of a blast event at a flat plate

The exponential rate of decrease of pressure as a function of time was proposed by Friedlander's equation [51], and is widely used in defining the pressure profile of a blast load, as:

Equation 1

$$P(t) = P_{op}\left(1 - \frac{t}{t_0^+}\right)e^{-\alpha\frac{t}{t_0^+}}$$

where P_{op} = peak overpressure (or incidence pressure); t_0^+ = blast duration of the positive phase; α = wave number, depends on P_{op} and chosen to yield a suitable impulse from the pressure-time relation; t = blast time; t_a = arrival time. For a specific stand-off distance (i.e. SD), in meters away from the charge, the peak overpressure is calculated as:

Equation 2

$$\frac{P_{op}}{P_a} = \frac{808\left[1 + \left(\frac{Z}{4.5}\right)^2\right]}{\sqrt{\left[1 + \left(\frac{Z}{0.048}\right)^2\right]}\sqrt{\left[1 + \left(\frac{Z}{0.32}\right)^2\right]}\sqrt{\left[1 + \left(\frac{Z}{1.35}\right)^2\right]}}$$

where Z = scaled distance, defined in equation form as a function of SD and charge weight W_e in terms of TNT equivalence:

Equation 3

$$Z = \frac{SD}{\sqrt[3]{W_e}}$$

The values of TNT equivalent constants could be obtained from books or manuals, such as from Karlos and Solomon [50]. The remaining parameter to be evaluated from the Friedland's equations is the positive duration of the blast t_d, and it was given by the equation:

Equation 4

$$\frac{t_0^+}{\sqrt[3]{W_e}} = \frac{980\left[1+\left(\frac{Z}{0.54}\right)^{10}\right]}{\left[1+\left(\frac{Z}{0.02}\right)^{2}\right]\left[1+\left(\frac{Z}{0.74}\right)^{2}\right]\sqrt{\left[1+\left(\frac{Z}{6.9}\right)^{2}\right]}}$$

All aforementioned survey on loading quantification is related to free-air bursts, where the shock wave has not been deflected or reflected by any surface during the propagation of the wave through air, this is called the incident pressure. Once the shock wave impinges to a surface and is reflected, the magnitude of the load on the surface multiplies by up to 20 folds of the incident pressure [9].

2.2.2. Scaling laws of blasts

One of the most reducing effect parameters to the properties of a blast wave is the distance from the blast source, so forth, scaling laws (Error! Reference source not f ound.) were used to predict the effect distance carried on the properties on the blast wave. Furthermore, the same laws could be used to predict the properties of a large-scale blast wave from smaller-scaled ones. These laws are known as the Hopkinson-Cranz [52,53] and Sachs [54], they were proposed during the 1st and the 2nd World War, respectively. Hopkinson-Cranz law suggests that when two explosives of the same material, geometry and medium conditions, but of different weight, are set at the same stand-off distance Z, then, both explosives will impinge a target surface with identical blast waves. Sachs law is suitable for different medium conditions of the explosive.

2.2.3. Blast load distribution

Once the shock wave arrives at t_a, two profiles are created on the top plate concerning the pressure load: the temporal (i.e. change with time) and the spatial (i.e.

change in domain) distribution profiles. Formulation of the load profiles is essential to give an understanding of the loading nature, and for running analytical and numerical analysis on the system of interest. It should be kept in mind that the load scenario highly affects the performance of the sacrificial structures. Therefore, a lot of care should be given into the algorithm used to describe the pressure load on the structures

Blast profiles behavior and interactions are complex, thus, commercial software packages based on blast load functions serve as a solution to this cumbersome issue. The code CONWEP (CONventinal Weapons Effect Program) is the most popular in the aspect of defining the blast load profile [55], equally effective, is the LS-Dyna package [56]. Both mentioned software work with the Kingrey and Bulmash [57] blast load function, which is given by:

Equation 5

$$P(t) = P_r \cos^2\theta + P_i(1 + \cos^2\theta - 2\cos\theta)$$

where P_i = incident pressure; P_r = reflected pressure; θ = angle of incidence (i.e. the angle between the tangent of the shock front and the tangent of the target's surface). Another highly effective software package is Ansys AUTODYN and is particularly designed for handling FSI (fluid-structure interaction) problems.

Loading profiles can be expressed by infinite number of terms in loading functions. Nonetheless, a number of research proposed a truncated series of one term, combining two independent parts [58,59], as follows:

Equation 6

$$P(r,t) = P_s(r)P_t(t)$$

where $P_s(r)$ = spatial pressure function; $P_t(t)$ = temporal pressure function. In the case of uniform loading, the pressure is distributed evenly across the structure's face, due to the normalized effect of the blast load, resulting in an assumption of a nullified spatial

distribution. Jacob et al. [60] mentioned that a uniform loading regime is associated with explosives in a stand-off distance exceeding the largest dimension of a plate, thus, a square profile is considered for Figure 2. Moreover, since impulsive loads' durations are very small, the temporal distribution could be cancelled out from the load-function, and a square-profile is considered in place of Figure 1, that is the exponential one [61].

It was already mentioned that two terms are what constructs the blast load relation $P_s(r)$ and $P_t(t)$ as shown in Equation 6. Furthermore, consensus was held by many researchers for the exponential decay profile of the spatial and the temporal functions [13,61,62], so forth, both of these profiles could be defined by the following functions:

Equation 7

$$P_s(r) = \begin{cases} P_0^+, & 0 \le r \le R_0, \\ P_0^+ e^{-m(r-R_0)}, & r > R_0, \end{cases}$$

and

Equation 8

$$P_t(t) = \begin{cases} e^{-bt}, & 0 \le t \le t_0^+ \\ 0, & t > t_0^+ \end{cases}$$

where r = radial distance from the top plate's center; R_0 = constant pressure radius; m and b = exponential decay constants of the spatial and temporal functions, respectively.

Theobald and Nurick [61] stated that since impulsive loading is adopted, the temporal-pressure distribution plays a less significant role than the spatial-pressure distribution. In their work, they assumed constant load over the blast time duration, and null beyond that. Moreover, pressure distribution was worked out in terms of the positive impulse (I) measured by the ballistic pendulum apparatus and re-arranged to give the following expression:

Equation 9

$$P_0^+ = \frac{I}{t_0^+\left[\pi {R_0}^2 + 8\int_0^{\frac{\pi}{4}}\left\{\frac{-e^{\frac{m(-hw+R_0 cos\theta)}{cos\theta}}(mw-cos\theta)+(1+mR_0)cos\theta}{m^2 cos\theta}\right\}d\theta\right]}$$

where w = the half width of the top plate; θ = angle of incidence, exclusive to non-uniform distributions, defined as the angle between the tangent lines of the shock wave and the top plate.

2.3. Structural crashworthiness and impact

Deformation behavior and energy absorption characteristics of structures are the traits of interest to accomplish the job as an efficient sacrificial panel structures. Sacrificial panels focus on an energy absorbing middle core structure; the core should be designed to initiate buckling and sustain deformation in a controlled manner. Structures subjected to a load stimulus behave dependent on a number of key factors: type of loading, strain-rates and inertia effects, with each being discussed in detail in the following sections.

2.3.1. Loading rate effects:

Researchers differentiate between quasi-static, dynamic and impulsive loading through the strain-rate ($\dot{\varepsilon}$) of deformed structures; impulsive loadings reach $\dot{\varepsilon}$ of $10^3 - 10^4\ s^{-1}$ with extremely small durations of loading [34]. This classification of loading rates is to differentiate between the deformation behaviors associated with the deformed structures. Strain and inertia effect of a crushed tube has an observable significance starting from certain loading rates, that is, dynamic loading, this is highly noticeable in axially loaded structures. For axially loaded thin-walled structures, lobe formation (i.e.

process of folding) is the inelastic deformation behavior of the structure to absorbing energy. Jones [8] adopted the behavior of thin-walled structures under quas-static loading as being undergoing mere progressive buckling of lobe formation. Moreover, with the same structures subjected to dynamic loading, they would develop compressive plastic strains along the whole length of the tube, causing the formation of dynamic plastic strains with a wrinkling pattern prior to the initiation of the lobe formation process. Therefore, it is clear from the defined deformation modes that dynamic buckling would tend to subject a bigger portion of the loaded structures to plastic deformation, which might be an idea of an increased energy absorbing capacity. This being said, researchers should be aware of the buckling stability that result in an overall reduction in the energy absorbed.

2.3.2. Inertia effects:

Upon loading a small-scale energy absorbing structure dynamically and scaling the results to a large model, the behavior will highly deflect from linear scalability [63]. This is due to the sensitivity of a big-scale structure to the axial and lateral inertias generated by inertia effects. Inertia effects may highly influence the peak load and the load-deflection curve, so, generally the collapse mode, depending on the structure's nature. Moreover, Calladine and English [64] identified two types of inertia-sensitive energy absorbing structures, from the course of their static-load deflection curve. Regarding the load-deflection curve, Type I: identified from a linear increasing load, then concaves downward to reside on a flat horizontal top, whereas, Type II: linearly increases, reaching a peak top load, then drastically drops in load. They justified this finding, by concluding that Type II structures were highly sensitive to the impact velocity, hence, inertia sensitivity, converse to the behavior of Type I structures which

are not inertia sensitive. Although the argument of inertia sensitive structures was studied initially on crooked plates, but, it is applicable to various thin-walled structures subjected to axial loading, such as, circular and polygonal tubes, and frusta tubes.

Further analysis on inertia-sensitivity was performed by Karagiozova et al. [65] by conducting experiments on circular thin-walled structures subjected to drop weights of different masses and velocities. The findings revolved around the significant influence of the impact velocity on the performance of the collapse performance of the crushed element. Furthermore, high-velocity impacts were found to cause dynamic plastic deformation, caused by the effects of the stress wave propagation manner (Figure 3). Additionally, the dynamic buckling results in a shortening phenomenon in the early stage of deformation, which contributes to a larger amount of energy absorbed in high-velocity impacts than low-velocity ones. This behavior was explained by the strains and stresses accumulated before buckling initiates, early in the deformation phase as mentioned earlier. It is worth noting that neither of the properties of elasticity, strain-hardening and strain-rate sensitivity have any influence on the performance of the inertia-sensitive structures [63].

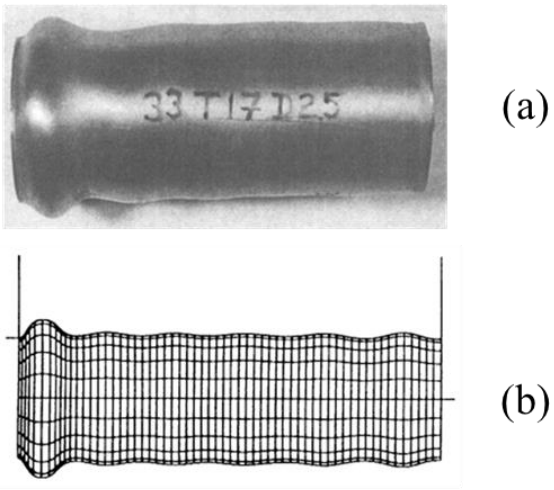

Figure 3. Dynamic plastic buckling of aluminum tubes (a) experimental specimen [66] (b) numerical simulation

2.3.3. Strain-rate effects

The mechanical properties of materials highly contribute to the performance of energy absorbers under impact, from a maximum displacement, transferred loads, and energy absorption point of view. Any variation in these characteristics, such as the ones responsible for the onset of permanent deformation or crushing load levels, will result in altering the behavior of the energy absorber. Various studies observed the effect strain-rate holds on metallic crushed members, where an increase in the yield strength and flow stress was observed. Jones [8] stated that material strain-rate sensitivity adds a strengthening factor to a structure, hence, it might act as a safety factor for the structure under load. It is worth mentioning that strain-rate sensitivity is a material property and is independent of the geometrical component of structures. Furthermore, Marsh and Campbell [67] conducted crushing tests on mild steel with different strain-rates and found that with the increase of strain-rate, although small increments were used, mild steel had shown significant strain-rate sensitive characteristics. Further strain-rate sensitivity experiments were carried for titanium, aluminum and magnesium

alloys [68,69]. Even though the aluminum and magnesium alloys displayed higher sensitivities than the titanium alloy, mild steel still showed the highest sensitivity to strain-rate.

As strain-rate effects played a significant role in determining the outcome of structures under dynamic loading, constitutive models were proposed to account for this character in deformation schemes. These models work on explicit analysis to determine the dynamic flow stress as a function of strain-rate of load. One of the most developed models is the Cowper-Symonds model [70], which works on adding a correction factor to the static flow stress to obtain the dynamic one. Due to the high reliance on this model for many materials under various applications, this empirical model was experimentally validated to assure the reliability of the results [71]. And, the mathematical form of the equation is the following:

Equation 10

$$\frac{\sigma_d}{\sigma_s} = 1 + \left(\frac{\dot{\varepsilon}}{D}\right)^{\frac{1}{q}}$$

where σ_d = dynamic stress; σ_s = static stress; $\dot{\varepsilon}$ = strain-rate, and, D and q = material constants.

A second common constitutive equation for the evaluation of the dynamic flow stress from its static counterpart is the Johnson-cook equation. Johnson-cook model covers a wide range of strain-rate, whereas, its major difference from the Cowper-Symonds model is the addition of the thermal softening effect to account for the temperature changes while undergoing plastic deformation of a structure [72]. The equation solves for the dynamic flow stress in terms of strain hardening, strain-rate strengthening, and thermal softening terms [73], and can be written in the following form:

Equation 11

$$\sigma_d = [A + B\varepsilon^n]\left[1 + C\ ln\left(\frac{\dot{\varepsilon}}{\dot{\varepsilon}_0}\right)\right]\left[1 - \left(\frac{T - T_{room}}{T_{melt} - T_{room}}\right)^m\right]$$

Where again σ_d = the dynamic flow stress, ε = the plastic strain, $\dot{\varepsilon}$ and $\dot{\varepsilon}_0$ = the strain-rate and the reference strain-rate, respectively. Furthermore, T = structural surface temperature, T_{room} and T_{melt} = the surrounding medium temperature and the material's melting point, respectively. The remainder are the five empirical parameters A, B, C, n and m, associated with the equation. Fortunately, it is a viable option to incorporate these models in finite element analysis packages as material models, for the full analysis of a system under high impact loading. Now, in the case of blast loads the stress wave arising while impacting a structure impulsively moves fast compared to temperature augmentation, accounting for the thermal softening term is of non-significance to the behavior, and is computationally expensive [74]. Therefore, the Cowper-Symonds is the model of choice in this thesis. An additional set of constitutive models accounting for strain-rate and thermal effects were reviewed by Liang and Khan [75], including the Bodner-Partom, Khan-Huang, and Zerilli-Armstrong models.

2.4. Structural basis for energy absorption

It is necessary to keep in mind that the most essential part responsible to carry energy absorption in a sacrificial panel would be the core of the panel, which are the thin-walled structures designed in this thesis. Performance assessment of thin-walled structures under impact is carried out by specific quantification equations and qualification measures. Therefore, before presenting the assessment methods in the following sections, an explanation on the general principles on energy absorbers is firstly introduced.

2.4.1. Fundamentals of energy absorbers

There are predetermined principles that are inclusive to all energy absorbing devices as discussed by Lu and Yu [63], despite the different structures' design and material selection to suit the different applications. These principles fulfill the purpose of an energy absorber, and that is to dissipate the kinetic energy of a colliding mass at a predetermined rate. The following sub-sections are to give a summary on the principles responsible for designing an applicable and efficient energy absorber.

2.4.1.1. Irreversible energy absorption

Irreversible energy dissipation has many forms, such as, plastic deformation, viscous deformation energy by friction, and, the fracture of excessively deformed thin-walled structure. It is worth mentioning that plastic deformation is the most efficient means of dissipating energy in ductile materials, and not forgetting that it has a wide practical range of applications. Plastic deformation happens on macroscopic and microscopic scales, such as, fold formation of crushed tubes, and the micro-cracks that take place in polymer-matrix laminates in composite materials, respectively. In order for energy absorption to take place, surpassing the elastic barrier has to happen for plastic deformation to initiate, and to store energy permanently. Failing to do so will result in the energy transferring across the system, affecting all components, including non-sacrificial structures and the occupants in that space. One reason to accomplish energy absorption efficiently is to decrease the amount of injury time available for the occupants.

2.4.1.2. Constant reaction force

The reaction force denotes the crushing force of the structure. It usually reaches a global or a local maximum upon reaching the elastic stress limit of the crushed element, after which plastic buckling initiates (i.e. yield stress). The value of the reaction force should be kept below a threshold in applications that concern the protection of a wall or a vehicle carrying occupants. Ideally speaking, the crushing force should be kept constant throughout the course of deformation to avoid the fluctuation of acceleration levels, thus, avoiding serious injuries.

2.4.1.3. Long stroke and confined space

Energy absorption is equal to the work done by the structure undergoing deformation, so forth, energy absorption is the multiplication of the reaction force by the displacement underwent by the deformed structure (i.e. stroke length), which should be maximized. Besides the concept of considering the reaction force values, analysis could be held in terms of the kinetic energy possessed by the colliding mass. As previously stated, the kinetic energy must be dissipated slowly to avoid excessive deceleration levels. For this to happen, Lu and Yu illustrated this concept with the words of ‘buying distance with time’. The idea behind these words is that the long stroke extends the time needed to bring the target to full stop, in return, the force levels are going to be reduced significantly. Although these words referred to individual sacrificial thin-walled crushed elements, an analogy of this concept using sacrificial panels was demonstrated by Paepegem [76] using a force-displacement graph as shown in Figure 4.

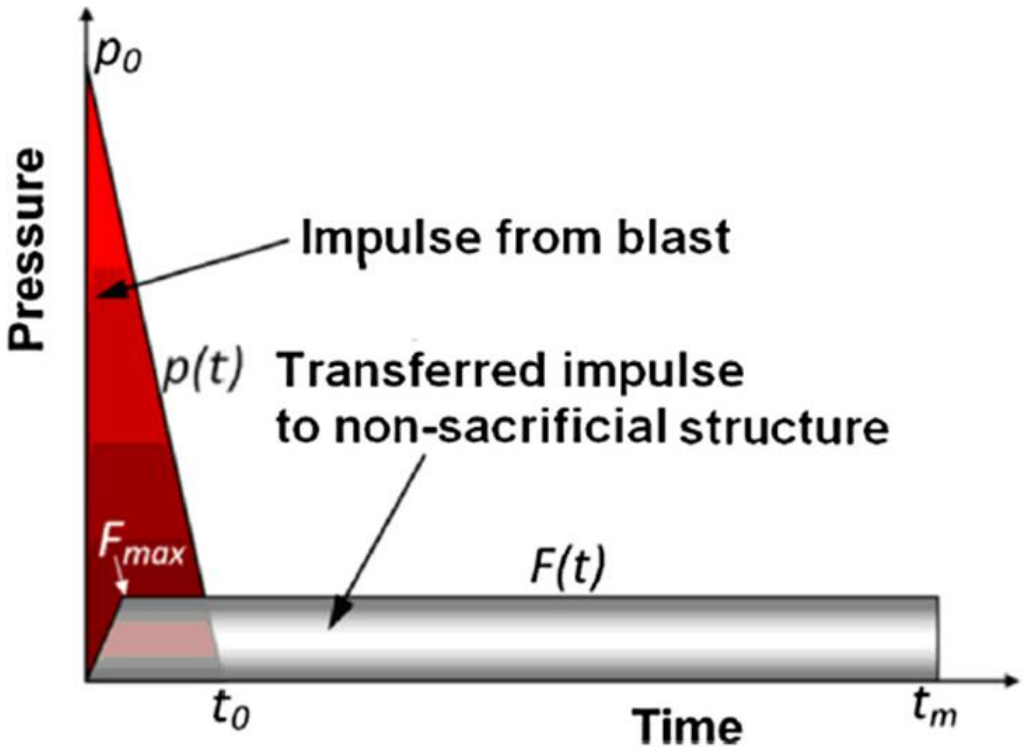

Figure 4. The working concept of sacrificial structures

2.4.1.4. Stable and repeatable deformation mode

Service crushing situations bypass different identities of the load encountering the sacrificial panel; majorly, the load comes carrying many uncertainties in its magnitude, direction and pulse shape. Therefore, designing aspects must focus on the idea of stability of a crushing member and repeatability of the efficient crushing mode under the possible different situations of loading. In other words, the sensitivity toward the mentioned uncertainties should be kept to a minimum, simultaneously, the energy absorbing capability of the structure should register consistency in the face of the different encountered situations. In this way the reliability of the structure will make it applicable in a wide range of applications.

2.4.1.5. Light weight and low cost

The weight of an energy absorber is a very important aspect to consider. Big weights of any object are associated with higher inertias, hence, higher resistance to bring a heavy fast object to full stop, and vice versa; this property is pinpointed at the top plate of sacrificial panels. Therefore, at the designing stage of energy absorbers, the designer should consider different materials and geometries to the structure, aiming to minimize the weight, while sustaining the energy absorption capacity at the same time.

Keeping in mind that as sacrificial panels are composed of many components, their price, highly probable, to be higher than energy-absorbing individual components. Furthermore, as sacrificial panels serve the purpose of protecting vital structures, these structures should be operated with economic limits, as to be affordable to all parties. This is particularly true since these structures are a one-time use; once consumed in a loading scenario they must be discarded and replaced with another.

2.4.2. Assessment of panel response

From a load-time point of view, the impulsive pressure from a blast is measured at a specific point from the blast source, starting at the P_0^+, then, reduces to the ambient atmospheric pressure in a near exponential manner. Furthermore, sacrificial cladding panels work on reducing P_0^+ experienced by the protected structure, by reducing the maximum peak pressure to a maximum peak force (PF) exerted on the back plate of the panel and extending the time of the impulse event. The post-buckling force is less than the PF, with a behavior of local peaks and troughs denoting the formation of fold's hinges. The performance of the sacrificial panel is assessed by several factors regarding the core tubes:

2.4.2.1. Deformation mode

The major deformation modes of previous axially blast loaded thin-walled core tubes were found to be progressive and off-axis (Euler) buckling, among the vast variety of deformation modes reviewed by Alghamdi [22]. The deformation mode of the tube denotes the buckling stability; hence, the attained energy by deformation.

2.4.2.2. Peak force (PF)

PF is the peak force representing the elastic stress limit of core tubes, after which plastic buckling initiates. It also denotes the maximum transferred load to the non-sacrificial structure if contact between the top plate and the back plate was avoided. Therefore, PF value must remain below the failure threshold of the non-sacrificial structure. In this study, the obtained peak forces were the initial in a force-displacement diagram. It should be kept in mind that that the forces transferred to the non-sacrificial structure are many folds higher in a plates' contacting condition than a non-contacting condition.

2.4.2.3. Maximum mean crush distance (δ)

The maximum crush distance underwent by the core tubes is measured as the difference between the initial and the final positions of the top cross-section’s middle point. An undeformed and deformed superimposition is shown in Figure. 5.

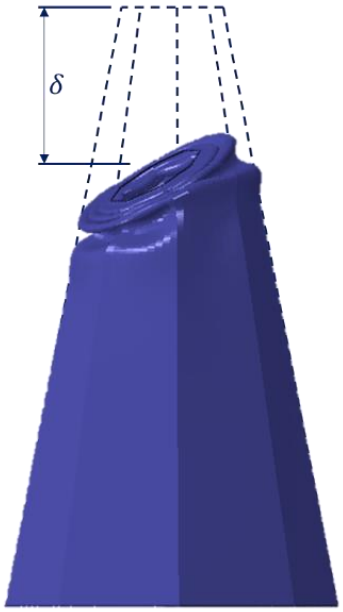

Figure. 5 Crush distance representation of a deformed tube

2.4.2.4. Stroke efficiency ($\boldsymbol{\varepsilon_{Stroke}}$)

$\varepsilon_{\mathrm{Stroke}}$ gives an insight of the tube's performance when subjected to crushing, showing the extent of tube's contribution to the energy absorption. $\varepsilon_{\mathrm{Stroke}}$ is a function of the maximum mean crush distance (δ) and the initial the undeformed length (L):

Equation 12

$$\varepsilon_{Stroke} = \frac{\delta}{L}$$

2.4.2.5. Energy absorption by the core (EA)

Energy absorbed by the core tubes is calculated by summing the area under the load-displacement diagram for all tubes (n_t) in a panel. The load is integrated from the undeformed position, up to the maximum mean crush distance of tube i, or until contact between the plates occur if it is the case. The load considered in the diagrams is the reaction force acquired from the fixed back plate:

Equation 13

$$EA = \sum_{i=1}^{n_t} \int_0^{\delta_i} F_i(u)du$$

2.4.2.6. Mean buckling load (P_{mean})

The mean load of buckling denotes the average value of the post-buckling load. Calculated by Equation 14, the ratio of the energy absorbed by tube i to the maximum mean crush distance by the tube:

Equation 14

$$P_{mean} = \frac{\sum_i^{n_t} P_{mean.i}}{n_t} = \frac{\sum_i^{n_t} \frac{EA_i}{\delta_i}}{n_t}$$

2.4.2.7. Energy Absorbing efficiency of the core (ε_{core})

The efficiency of the core measures the extent of core contribution to energy absorption with respect to the panel subjected to the impact loading. It is calculated from the ratio of energy absorbed by the core to the work applied to the system (W):

Equation 15

$$\varepsilon_{core} = \frac{EA}{W}$$

2.5. Sacrificial cladding structures

Thin-walled members are a key component in the designing stage of a sacrificial panel. An effective solution to enhance the energy absorbing characteristics of a panel, is to start with the thin-walled members in the core. To fully understand the behavior of sacrificial panels in action, a fully integrated structure needs to be implied and tested against a real-life blast, added to it the medium disturbances associated with the loading.

However, researchers studied each component of a sacrificial panel individually in action. This is due to the enormous amount of resources needed to carry out the experiment, and the extensively long computational time needed with respect to the numerical-based studies. Analyzing the split portions of a panel would give a good indication of the panel's performance, given the constraints of cost and time.

2.5.1. Air blast-loaded plates

The first class of blast resistant entities that took into account the characteristics of compactness, mass, strength and stiffness-to-weight ratio were individually loaded plates [1]. In addition, recent studies aim for ceramic and polymeric based composite materials, due to their high stiffness-to-weight ratio, whereas, earlier studies focused on wholly metal plates. The two major studied geometries of monolithic plates were circular and square flat plates; the addition of stiffeners, observed in research work, is to decrease the deformation displacement resulting from the blast loading.

2.5.1.1. Metal monolithic plates:

Furthermore, Jacob et al. [77] studied the influence the external load and the plate's geometry has on monolithic plates, and, a similarity was observed in the deformation scheme for square and circular monolithic plates (Figure 6). Moreover, despite the significant influence boundary conditions of the clamping method and the distribution of applied load has on the response of metal plates, but, the failure progression can be generally defined by three failure modes: large plastic deformation, tensile tearing and shearing. Non-dimensional analysis was the main concern for researches in assessing the response of monolithic plates under deformation pattern. Non-dimensional models hold the ability to compare experimental results of panels

with different scales, different loading conditions and material properties. Prior to proceeding with the non-dimensional analysis, it is worth mentioning that all the following empirical equations are exclusive to mild steel monolithic plates, which are known to be highly strain-rate sensitive.

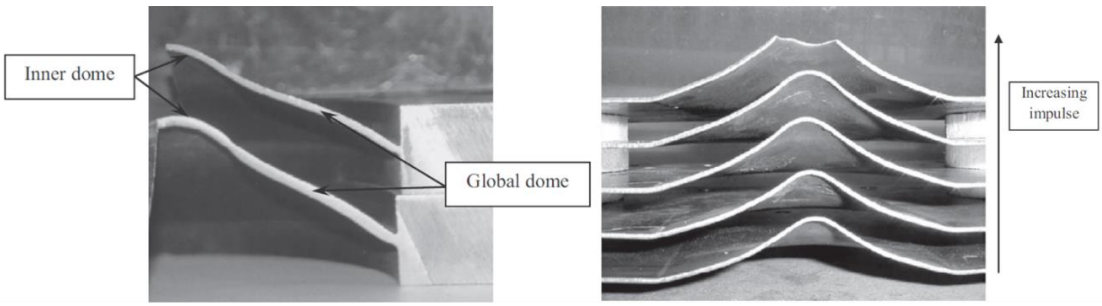

Figure 6. Localised load at (a) two built-in circular plates (b) quadrangular plates [78]

Nurick and Martin [79] proceeded with the work of Li and jones [80] to identify a dimensionless number by carrying non-dimensional analysis to quantify the response of tubes under blast loading. The deflection of plates being one of the most important parameters used to assess the performance; their final aim was to model a constitutive equation that would estimate the response of any circular or square plate subjected to an air blast load, using dimensionless parameters. The modeled equations quantify the large inelastic displacement only, provided that the plates prevent suffering from tearing or shear failures. Dimensionless damage numbers: $\varphi_c =$ non-dimensional impulse parameter for circular plates, and, $\varphi_q =$ for quadrangular plates were proposed, which will be further discussed on, displayed in the following equations:

Equation 16

$$\varphi_c = \frac{I}{\pi R t^2 (\rho\sigma)^{\frac{1}{2}}}$$

Equation 17

$$\varphi_q = \frac{I}{2t^2(BL\rho\sigma)^{\frac{1}{2}}}$$

Where $I =$ impulse; $R =$ exposed plate radius; for quadrangular plates, $B =$ plate breadth and $L =$ plate length; $t =$ plate thickness; $\rho =$ material's density; $\sigma =$ material yield stress. Finally, the damage dimensionless parameters were related analytically to the plate's response by the mid-point deflection-to-thickness ratio δ/H. These models are applicable for circular and quadrangular plates incorporating equal cross-sectional area, material and thickness properties, being subjected to uniform impulsive loading. The ratio of Equation 16 to Equation 17 is used to obtain the final parameters for the equation $\frac{\delta}{H} = f(\varphi_q)$ as:

Equation 18

$$\frac{\varphi_c}{\varphi_q} = \frac{2}{\pi^{0.5}} = 1.128$$

Equation 19

$$\frac{\delta}{H} = 0.48\varphi_q + 0.277$$

Nurick and Martin's work, worked well for uniformly loaded plates, but, had a misleading information when it comes to close-range blasts. Therefore, Jacob et al. [77] studied the effect of load-localization on quadrangular tubes. Afterwards, Jacob et al. [60] carried further research to study the effect of stand-off distance on the load-localization on clamped circular tubes. Jacob's experiments covered circular discs that are 106 mm in diameter, and the studied stand-off distances away from the blast source to the plate's center ranged from 25 – 300 mm. From 25 – 40 mm the load was localized, from 40 – 100 mm the load was described as being in a transition loading regime, and obviously, the load would be defined uniform above that stand-off. As a result, it was

concluded that a uniform loading regime is associated with explosives in a stand-off distance exceeding the largest dimension in a plate. Although the strain-hardening and the strain-rate effects of the materials were not mentioned in all aforementioned equations, their effects are embedded.

Moreover, due to these findings on load-localization and stand-off distance, Jacob [60] modified upon the damage parameters of Nurick and Martin [79]. The effect of load localization to quadrangular plates in close-range blasts were added by multiplying the dimensionless number φ_q by the loading parameter '$1 + \ln\left(\frac{A}{A_0}\right)$'; where the plate area $A = BL$; the charge area $A_0 = \pi R_0^2$, as a function of the charge diameter R_0. Similarly, the effect of stand-off distance on the dimensionless number φ_c was added to circular tubes, by multiplying φ_c by '$\frac{1}{1+\ln\left(\frac{S}{R_0}\right)}$'; where S=stand-off distance. A final regression analysis performed by Yeun [78] on a bigger population of air-blast loaded plates, reaching a correction factor being added to the previous equation, claiming that it provided a better response prediction:

Equation 20

$$\frac{\delta}{H} = 0.446\varphi_q + 0.261$$

2.5.1.2. Composite plates

Currently, researchers have given their effort and focus to composite plates, due to their high stiffness-to-weight ratio and their multiple energy dissipation mechanisms. These plates undergo brittle failure with layers delamination, fibers breakage and matrix cracking [21], which could be rendered beneficial in the field of blast mitigation.

Despite composite materials holding such beneficial characteristics, the conventional material of use for the panel's top plate is mild steel. This revolves around

the fact that the knowledge on mild steel is complete. Also, it is easy to manufacture due to the fully developed production technology, resulting in a lower production cost, despite mild steel being dense. Furthermore, mild steel possesses strain-rate sensitive characteristics, which are registered as highly effective characteristics under impact loadings.

2.5.2. Sacrificial cladding members

Monolithic plates on their own are heavy adding them to protected structures. That is due to the big thickness needed against blast pressures [81]. This is an adequate reason for researches to steer away from monolithic plates to sacrificial cladding structures. Research focus had been directed toward tubular lightweight cores in cladding structures because of their capability to carry transverse loads with minimal weight penalty, and, absorbing large amount of plastic energy. In which tubular structures as core in claddings are now becoming more popular for blast mitigation applications, including ship hulls, armored vehicles, buildings' claddings, etc. As previously mentioned with thin-walled members being the key component to absorbing energy, this section presents a brief review on laterally loaded cores, and, focuses more on axially loaded cores under dynamic and impulsive loading.

2.5.2.1. Tubular structures with lateral placement

Laterally loaded tubular structures easily sustain stability while undergoing crushing, this answers the question of 'why most studies focus on core structures with smalls height in cladding structures?'. Recently, Xia et al. [28] studied the energy absorption characteristics in sandwich structures with the lateral placement of the circular core tubes. Three configurations were examined in their analysis: three-tubes

core, four-tubes core and five-tubes core, for a fixed overall width of the panel (while changing the spacing between tubular elements). Along swapping between the panel configurations, changing the top plate thickness, tube wall thickness, mass of TNT, and stand-off distance was carried out for each panel configuration. For close-ranged blasts, Xin recommended the no core-spacing panels (i.e. five-core tube), with the deformation being exclusive to top skin tearing and core crushing. On the other hand, panels with the core spacing (i.e. three- and four-tubes core) produced an unfavored response, that is being back skin tearing. For contact explosion scenarios, the top skin responded by forming corrugations, with the core tubes left intact, therefore, a recommendation was given to the usage of three-cores panels due to their smaller stiffness. Yuen et al. [78] extended Xin's work by incorporating smaller charges, uniform loading conditions, core spacing, and different tubular structures (empty or foam-filled). An indication of an enhancement in the performance of core tubes that are constrained with no gaps between the adjacent elements was observed. This behavior was emphasized on by Shim and Stronge [82], which was explained by the development of extra hinges due to the constraining of the tubes, thus, will result in an enhancement in the energy absorbing characteristics. Yuen added fillings on, concluding that fillers did not affect the deformation mode, but, might enhance energy absorption depending on the foam's characteristics, if it possesses high plateau stresses, then, energy absorption increases, and vice versa.

On the other hand, recent research studied different cross-sections of cores. Xiang et al. [10] studied circular and square cross-sections, Zhang et al. [29] studied corrugated cross-section, and Jin et al. [83] studied an innovative auxetic re-entrant honeycomb core structures. Xiang et al. [10] mentioned that over half of the applied energy was dissipated by local deformation of tubes, and the rest was dissipated by

global flexural bending deformation, emphasizing on the local deformation terminating before global deformation even started. Additionally, square and circular core tubes performed similar to each other, and performed better than monolithic plates under small blast loads. Zhang et al. [29] examined empty and different foam-filling strategies: back filling, front filling, and fully-filled corrugated core tubes. The fact that different filling strategies were implemented had shown a difference in the energy absorbing characteristics, with the front side filling possessing the highest blast mitigating and energy absorbing effects. Jin et al. [83] considered many design enhancements aside from the innovative cellular cross-section. Multi-layers of the repeating cross-sections were placed in a parallel- and a cross- arrangement, furthermore, functionally graded thicknesses across the layers were proposed. The configuration of the cross-arranged panel with the core top possessing a higher thickness than the descending layers resulted in the best performance among all others.

2.5.2.2. Tubular structures with axial placement

Axially loaded members, on the other hand, were found to absorb ten folds of energy during progressive buckling compared to laterally loaded structures [22]. This is due to the majority of the material deforming plastically to participate in the energy dissipation process [27]. But, the biggest constraint with this placement is the buckling stability of the tubes under the different loading situations, especially when the tubes are subjected to oblique impacts. There is an extensive amount of research of axially loaded members under quasi-static and dynamic loading, whereas, relatively speaking, much less research was held for blast loaded members. Afterall, the energy absorption behavior and deformation modes of the various cross-sections and configurations under all loading situations is discussed in this section.

I. Circular tubes

i. Quasi-static and dynamic loading

Circular tubes registered excellent energy absorption characteristics with respect to other cross-sections, hence, a lot of research adopted them for axial loading conditions [71,84]. Different deformation modes where registered under pure axial crushing, and that is axisymmetric concertina mode (i.e. ring mode), non-symmetric mode (i.e. diamond mode), and mixed mode which encompasses the first two as shown in Figure 7a-c [85]. Additionally, members could undergo a fourth deformation, which is the global-bending (i.e. non-compact mode), shown in Figure 7d. It is essential to mention that among the four deformation modes, the ring mode is considered the most stable one, associated with the maximum possible energy absorption. Furthermore, as an energy absorption assessing tool, circular tubes were found to register a stroke efficiency (ε_{Stroke}) ≈ 0.75, which is higher than that of square tubes, as will be shown in the following sub-section [8].

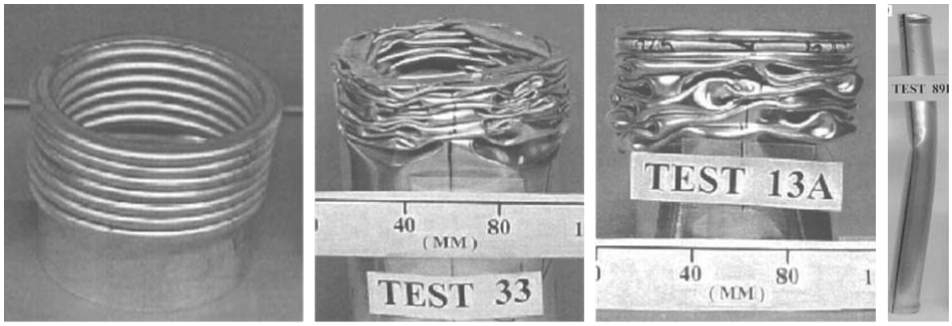

Figure 7. Main deformation modes of circular tubes under axial static loading (a) axi-symmetric (b) non-symmetric (c) mixed mode (d) non-compact mode

Significant influence of the geometrical parameters was directed toward the deformation modes aforementioned. Furthermore, researchers emphasized on studying dimensionless parameters, to ease the scaling aspect of structures. Therefore, two geometries were proposed and found to construct a basis for the deformation modes perfectly: the ratios of diameter to thickness (D/t), and Length to thickness (L/t) (Table 2).

Table 2. Deformation Modes of Circular Tubes in Accordance to their Dimensionless Geometrical Parameters

Diameter/thickness & Length/thickness	**Deformation mode developed**
$\boldsymbol{\frac{D}{t} < 50}$ & $\boldsymbol{\frac{L}{t} < 2}$	Ring mode
$\boldsymbol{\frac{D}{t} > 80}$	Diamond mode
$\boldsymbol{\frac{D}{t} < 50}$ & $\boldsymbol{\frac{L}{t} > 2}$	Mixed mode

Researchers used the obtained experimental results to construct theoretical equations that would predict the mean force P_{mean} of a crushed tube, where they work on assessing the efficiency of energy absorption. A collection of research developed P_{mean} equations for the different deformation modes, such as axi-symmetric [84], and asymmetric [86]. For quasi-static axial loading, Guillow et al. [85] worked an empirical equation that predicts P_{mean} as a function of D/t under all deformation modes:

Equation 21

$$P_{mean} = 18.075\sigma_0 t^2 \left(\frac{D}{t}\right)^{0.32}$$

Where $\sigma_0 =$ the yield stress of the material. Moreover, the empirical equation of P_{mean}

for circular tubes undergoing axi-symmetric buckling under axial dynamic loading was developed, taking the strain-rate effects into account using the Cowper-Symonds equation [8]:

Equation 22

$$P_{mean} = \frac{2(\pi t)^{1.5} R^{0.5} \sigma_0 \left\{1 + \left(\frac{V_0}{4RD}\right)^{\frac{1}{q}}\right\}}{3^{\frac{1}{4}}}$$

Where V_0 = impact velocity. It is worth mentioning that this equation is accurate when the attached mass is much larger than the mass of the tubular element.

ii. Impulsive loading

An experimental and numerical analysis was carried out by Karagiozova et al. [74] to study the behavior of transmitting axial explosive loads through an attached mass (acting as a top plate) to circular thin-walled tubes (Figure 8). Prior to buckling, an initial compressional phase resulted in the creation of asymmetric wrinkles along the tube, which is analogous to the dynamic plastic buckling of tubes mentioned in Section 2.3.2. The initial compression phase phenomenon was significantly noticed particularly during the use of relatively small inertia of the top attached mass. The initial compression phase absorbed a significant amount of energy, hence, leaving less energy for the progressive buckling of the tube, thus, resulted in a less deformed length. In the end, the total amount of energy absorbed was higher than a quasi-static or impact events. That was due to the strain-rate effects taking place and increasing the resistance load on the tubes.

Figure 8. Deforamtion mode of axially loaded circular tubes under blast load [74]

Palanivelu et al. [76] studied the performance of single empty metal cans against blast loading, experimentally and numerically. In these tests of can crushing, the researchers did not intend to unify the kinetic energy of the top plates, rather, the attained energy by the skin plates for cans crushing was much less for plates of higher inertia. Therefore, plates with higher inertia resulted in a much less deformation. Paepegem et al. [62] conducted experimental and numerical tests on the behavior of single blast loaded composite tubes, and, upgraded them to sacrificial panels with an axial array of the same previously tested tubes. Suggestions on the use of high bending stiffness for the rear skin, and, a top skin with a small mass were given.

II. Square tubes

i. Quasi-static and dynamic loading

Square tubes acted as an elementary solution to the difficulty of mounting circular tubes to other structures. An issue arose in square tubes being less energy

absorbing efficient than circular tubes. An approximation of square tubes being 0.7 as effective as their circular counterparts [87]. This could be due to the fact that square tubes concentrate a lot of the deformation in the corner regions, which is the compressive strain, as highlighted by Karagiozova et al. [74]. Again, square tubes, as circular tubes, deform in a predetermined manner under the application of axial loading. Also, three deformation modes were registered: extensional, in-extensional, mixed mode, and non-compact mode [8,27]. Furthermore, as an energy absorption assessing tool, square tubes were found to register a stroke efficiency ($\boldsymbol{\varepsilon_{Stroke}}$) = 0.73, which is less than that of circular tubes. Moreover, the deformation mode highly depends on the dimensionless parameter width to thickness ratio (b/t). Table 3 reviews the values of b/t corresponding to the specified deformation modes.

Table 3. Deformation Modes of Square Tubes in Accordance to Their Dimensionless Geometrical Parameter

Width/thickness	**Deformation mode developed**
$\boldsymbol{b/t < 7.5}$	Extensional mode
$\boldsymbol{b/t > 40.8}$	Inextensional mode
$\boldsymbol{7.5 \leq b/t \leq 40.8}$	Mixed mode
$\boldsymbol{b/t = 100}$	Non-compact mode

Similar to the case of circular tubes, scientists arose interest in developing a general theoretical equation for estimating the mean crush force P_{mean} for axially crushed square tubes, regardless of the mode of deformation. Abramowicz and Jones [84] worked on estimating P_{mean}, while considering the strain-hardening effect of the material to obtain a better estimated solution:

Equation 23

$$P_{mean} = 13.06\sigma_0 b^{\frac{1}{3}} t^{\frac{5}{3}}$$

for the case of dynamic loading, Jones [8] worked on accounting the strain-rate effect component:

Equation 24

$$P_{mean} = 13.06 b^{\frac{1}{3}} t^{\frac{5}{3}} \sigma_0 \left\{ 1 + \left(\frac{0.33 V_0}{bD} \right)^{\frac{1}{q}} \right\}$$

it is worth mentioning that this equation is accurate when the attached mass is much larger than the mass of the tubular element.

ii. Impulsive loading

Under the process of blast loaded thin-walled tubes, circular tubes performed slightly different than that of square tubes as observed by Karagiozova et al. [74]. Additionally, the response of square tubes subjected to high-velocity impact is totally different than the low-velocity counterpart. Shell wall thickening was a significant phenomenon. due to the initial compression phase and the post-compression that took place during folds formation along the whole buckling phase. Compression at the corners of the square tubes accounted for the main energy absorption mechanism, rather than folding, resulting in severe thickening, even at the shell walls.

Theobald and Nurick [34] ran a numerical study on sacrificial panels confining axially placed square tubes as core. Optimizing the panels' performances was their aim, as they enhanced the buckling stability under uniform blast loads. The tubes were positioned according to a parameter $\lambda = \frac{\lambda_1}{\lambda_2}$. λ represents the ratio of the distance from the panel center and the axis of the tube, to the distance from the panel's center and

corners of the top plate. The author mentioned that in real-life blast events the top plate deforms, because of the relative low bending stiffness [76]. This implies a bending moment on the core tubes, affecting their stability, as this resembles an oblique loading on the tubes, resulting in global bending. Therefore, an optimal tube positioning was obtained for each of the three panel configurations studied, resulting in a nearly perfect axial progressive buckling response, λ = 0.528 for four core tubes; λ = 0.613 for five core tubes; λ = 0.698 for nine core tubes.

Theobald and Nurick [61] were proceeding from their previous numerical work [34], to experimental work, to fully assess the buckling behavior of the tubes. It was found that for relatively small impulses, not using the full stroke, irregular buckling modes were observed. While, for impulses that use the full stroke of the core tubes, symmetric buckling modes were the result. In the same study, Indentation triggers were used at the mid-span along the tubes, but, seemed that buckling initiation was not affected by these triggers, claiming that the indentation depth was not enough to initiate buckling in that location. Although triggers are sufficient to induce buckling at specific locations under quasi-static events, this is not the case under dynamic buckling. This might be due to the inertia effect and the heterogeneous material properties arising from strain-rate effects of the material along the structure [74]. An analytical solution was proposed for the top plate-core displacement ($u_t(t)$) of sacrificial panels with square core tubes under blasts:

Equation 25

$$u_t(t) = \begin{cases} 0, & t \leq 0 \\ V_0 t - \dfrac{n_t P_{mean} t^2}{2 A_p \rho_p h_p}, & 0 < t < t_m \; and \; t < t_c \\ Sl, & t \geq t_c \end{cases}$$

where t = time; n_t = number of tubes in the core; A_p = top plate exposed face to blast;

ρ_p = top plate material density; h_p = top plate thickness; t_m = total panel response duration; t_c = compaction time (i.e. consolidation of folds or contact of top plate with bottom plate).

III. Outward and Inward cornered tubes

Since thin-walled structures had a promising energy absorption characteristic, and the observation that square tubes focuses their deformation near the tube's corners, researchers extended their field of vision to study polygonal tubes. Rossi et al. [88] claimed that an increased number of walls in polygonal tubes, under axial collapse, leads to a higher plastic deformation, hence, resulting in a higher energy absorption and a smaller permanent displacement. Most studies comparing the performance of polygonal tubes numerically found that hexagonal and octagonal sections registered the highest enhancement for energy absorption [72,89]. Where one the findings were about hexagonal and octagonal cross-sections absorbing the highest amount of energy, among other polygonal cross-sections, against axial and oblique loading, respectively. For that case, P_{mean} theoretical equations of quasi-static axial crushing were worked out for hexagonal tubes [90]:

Equation 26

$$P_{mean} = 20.23\sigma_0 b^{0.4} t^{1.6}$$

and octagonal tubes [91]:

Equation 27

$$P_{mean} = 9.806\sigma_0 b^{0.5} t^{1.5}$$

Similarly, as mentioned in Section 2.5.2.2 – II, cornered tubes have common progressive deformation modes: extensional, in-extensional, mixed mode, added to

them the square mode of collapse [92]. In contradictory to square tubes, the mixed mode of deformation results in the maximum energy absorption [93]. Deformation modes of polygonal tubes were found to depend on the angle between the side walls of the structure (i.e. cross-sectional angle) by the trend shown in Table 4 [94].

Table 4. Deformation Mode of Polygonal Tubes

Cross-sectional angle	**Deformation mode developed**
$\boldsymbol{\theta < 90^\circ}$	In-extensional mode
$\boldsymbol{\theta \geq 120^\circ}$	extensional mode
$\boldsymbol{90^\circ \leq \theta < 120^\circ}$	Mixed mode

Generally speaking, no difference in the energy absorbing characteristics of tubes beyond 11 corners [95]. So forth, as a solution to the maximum number of corners on tubes, research suggested introducing inward corners, such as star-shaped [96] and criss-cross sectional tubes. The criss-cross and the star-shaped cross-sections produced a higher energy absorbing efficiency when compared to polygonal cross-sections.

IV. Surface patterns & Triggers

When referring back to Section 2.3.2 it was shown that the type II inertia-sensitive-structures start their plastic deformation at an initial peak force. This implies a desirability to avoid the high deceleration levels on the base structure. Triggers or imperfections had served the purpose of reducing the peak crushing force of structures, raising the initial stresses prior to crushing [97]. Furthermore, triggers could be used to serve the purpose of altering the deformation mode of crushed members; they could encourage a symmetric deformation mode by outperforming the other mode. Circular

cut-outs where introduced to axially loaded members, being found that they exhibit lower initial peak forces. If global deformation is to happen, they would increase the displacement of the structure before that [98].

Theobald and Nurick [61] faced some obstacles with the circular cutout triggers, where it was found for a very small sizes of the cutout the buckling mode would not be affected, while, very big sizes causes ductile fracture (i.e. tearing) that surrounds the perimeter of the hole. To prevent such a problem, the cutouts where replaced with small dished indentations, produced with a hemispherical indenter. Other types of triggers would be the corner indentations; triggering dents; corrugated tubes; parallel sharp dents at the side of the tube; parallel side dents at the side of the tubes, which were all reviewed by Yuen and Nurick [31].

V. Tapered tubes

All of the previously mentioned buckling modes of thin-walled tubes were a result of a perfect axial crushing of the tube; axial loading is an ideal assumption when it comes to real-life events. Tubular structures are subjected to oblique loadings when the impact is applied at an angle, and, it occurs to sacrificial panels when the bending stiffness of the top plate is low enough against the load. Oblique loading is much cumbersome than axial loading, because the Euler failure mode is more probable of occurring in the former event. Euler buckling must be avoided as it hinders thin-walled structures from utilizing the full deformed stroke, hence, resulting in a much less absorbed energy (Figure 9).

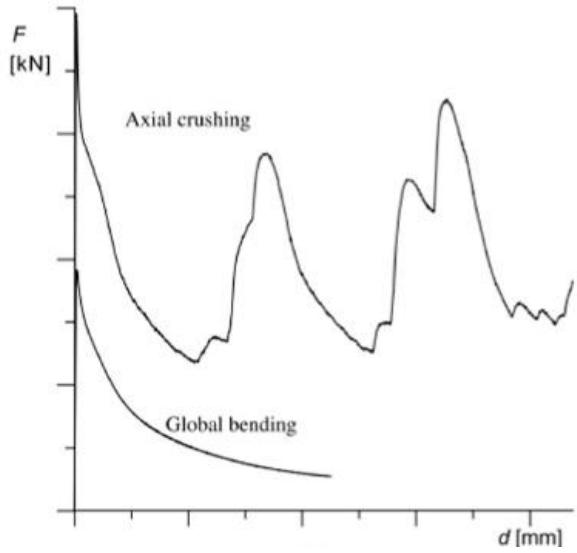

Figure 9. Typical force-displacement diagram for progressive and global bending of extruded members

Previous studies on thin-walled tubes had shown that Euler buckling is a possibility under axially loading as well. Circular and square tubes have specific values of the dimensionless parameters aforementioned in Table 2 & Table 3 (D/t and L/t for circular, and, b/t for square) that when exceeded Euler buckling is the result [85]. Further analysis had shown that a critical length (L_{cr}) phenomenon exists; when the crushed member is shorter than L_{cr}, progressive buckling is the result; when at or near the threshold, mixed-global mode is the result; exceeding L_{cr} would result in global buckling [99]. Moreover, L_{cr} was found to be dependent on the dimensionless parameters; tubes with a bigger dimensionless geometrical parameter, L_{cr} was found to be longer. L_{cr} was also found to be increasing with the impact velocity of the load [100].

To fully address the issue of oblique loading, tapered tubes were considered to be preferable to straight tubes as they perform similarly under axial impact, but more efficient under off-axis impact [101]. This performance is true for quasi-static and

dynamic loading, where tapered tubes are more resistant to global buckling than straight tubes. Although tapered tubes have a smaller specific energy absorption (i.e. energy absorbed per unit mass) than straight tubes [102], but, this is compensated from the higher resistance against Euler buckling. Due to the difference in geometries between the tapered and the straight tubes, additional parameters were used to assess the energy absorbing behavior of tapered tubes. Namely, these parameters are the taper angle, number of tapered sides, and the length and thickness [35,44]. From a deformation mode point of view, tapered tubes deform in the three modes aforementioned: axisymmetric, asymmetric and mixed mode [103].

It is worth mentioning that tapered tubes are no different from straight tubes, where similar studies to the conventional tubes were held for the tapered ones. The effect of the different cross-sections on tapered tubes were studied and analyzed by Guler et al. [44]. Else again, circular tubes ranked the top from a deforming stability and energy absorption point of view. Triggers of circular cutouts, circumferential dents and corrugations were also studied [33,45–47]. Triggering had shown the same potential as collapse initiators in tapered tubes as it did in the conventional case. Finally, the number of tapered sides was found as an influential parameter in determining the buckling behavior of tubes [104].

2.6. Finite element analysis (FEA)

From decades to hitherto analyses were mainly held by two frequently used methods: experimental and analytical. A new and one of the most used methods to analyzing the behavior of thin-walled structures is finite element analysis. A lot of research had focused on running this latter method due to the decrease amount of resources and the reliable ways of assessing the performance of analyzed systems.

Afterall, finite element modelling and analysis is the adopted method to run the work of this thesis.

2.6.1. Modelling of sacrificial panels

The finite element packages had been considered by many researchers as powerful tools to solve the problem of crushed core components of sacrificial cladding structures. They can be used to visualize the non-linear dynamics for large velocity impacts, that are cumbersome except by special instruments that are not readily available. The codes of finite element packages adopt an iterative approach of complex analytical models based on meshed systems (building blocks). These are extended to run parametric studies to assess the system in hand under different boundary conditions, loading events and geometrical components of the system. A vast number of finite element tools are available to accomplish the job of assessing the behavior of blast loaded members, some of these are LS-DYNA, AUTODYN, ABAQUS and ANSYS. ABAQUS is a readily available software, has a user-friendly interface, and is fully capable of running the job in hand. Therefore, the non-linear finite element package ABAQUS/Explicit is the software of use to simulating the buckling behavior and assessing the energy absorption performance of sacrificial panels subjected to blast loading.

2.6.2. Literature related FEA

Numerous amounts of studies had been published on the assessment of the performance of structures with the help of FEA. This analysis method works on detecting the behavior in complex situations that are not possible with the application of theoretical equations. For FEA to be a reliable source of data, validation of the model

is essential prior to running the analysis, doing so would result in mimicking the real-life physics of the response to a large extent. It should be noted that even this approach holds some drawbacks, where, sacrificing time is an issue, as this method uses more mesh (i.e. block of an analysis domain), for a higher accuracy. Therefore, an optimization of the time against the accuracy of the results is to be done through a mesh sensitivity study, which will be discussed in the next chapter. For the time being, numerical studies found in literature will be displayed to show the reliability of this analysis method.

It should be noted that when it comes to deformation of crushed members, two responses are to be expected, the local and the global deformation behavior. There were some cases, that the local behavior of deformation was not accurately predicted by FEA, but, the global deformation was [61]. Nevertheless, the behavior would be adequately described by numerical means, resulting in a reliable source to assess the energy absorption of structures. Figure 10 depicts a number of the numerical models of thin-wall members subjected to impulsive loading, and their experimental counterpart [74,76,105]. It can be shown from the figure that in some cases the deformation is not exactly mimicked by the simulated models, but nonetheless, the results are adequately accurate to define the response underwent by the blasted members.

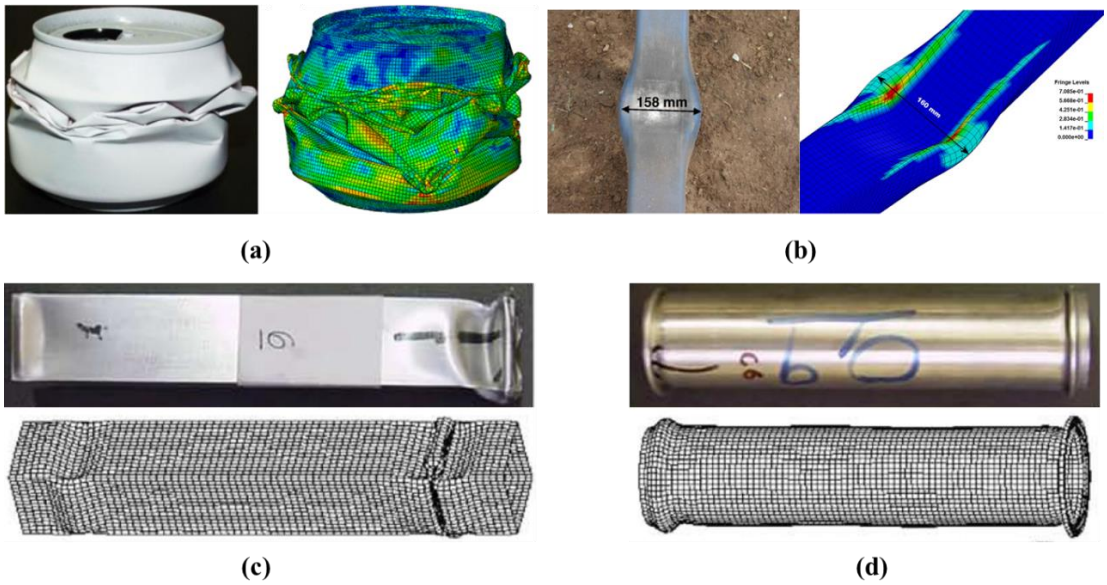

Figure 10. Examples on numerical models and their experimental counterparts

Jin et al. [106] numerically studied sandwich panels with a honeycomb cellular core subjected to impulsive loading. Since Jin's work is on cellular structures, observing their deformation was cumbersome, thus, the numerical methods were able to shed light on sensitive areas, where the deformation was fully analyzed. Jin's accomplishment is an enhancement of a previously published work of a validated numerical model and its experimental pair [107,108]. In addition, finite element methods is fully capable of simulating heterogenous material properties, such as the work done by Paepegem et al. [62], which had again proven beneficial for defining the deformation regime that was hard to detect experimentally.

From what was shown above about the accuracy of predicting crushed members' responses by FE packages, it is a good measure to consider finite element methods for analyses. This is especially true in blast loading events, where running such experiments would need certain governmental approvals, and specific equipment that are hard to afford in certain countries. Therefore, Finite element analysis is the adopted technique to model and assess the performance of sacrificial panels in this thesis. Not

to forget that validation of the model prior to testing was taken into account, to assure the accuracy of the acquired data.

2.7. Literature review summary

It was deduced from the reviewed literature that the topics focused on blast loaded members. In sequence, the topics reviewed in particular were the physics of blast waves, structural impact, fundamentals of structural energy absorption, sacrificial panels' components and their analysis, and finite element methods for carrying impulsive impacts on sacrificial structures.

2.7.1. Main findings

It was shown than a near full understanding of the physics of blast loading was revealed, and various consecutive equations were found to define the loading situation held by impulsive load-producing devices. With the help of commercial packages, loading situations were accurately mimicked for the impact of sacrificial structures, and a reduced cost than experimental means. Furthermore, the review had revealed than an extensive amount of research had directed the focus toward impulsive loaded members, with transverse placement of the members in particular. conversely, much less work had been directed toward the axial placement of members subjected to impulsive loading. Moreover, with localized loading being the main focus of this thesis, near-field blasted top plates showed oblique loading characteristics, which are harder to deal with than axial loads. That being said, it was shown that tapered members possess appealing characteristics against oblique loading in comparison to straight tubes. Furthermore, while there are a number of researches that dealt with circular and square cross-sections of thin-walled straight tubes, but, limited studies were conducted on polygonal tubes

under high strain-rate loading situations. Also, octagonal cross-sections being in the polygonal category, they displayed excellent and one of the best energy absorption characteristics under oblique loading. So forth, depending on the previous reasoning, octagonal tapered tubes might register enhanced energy absorption characteristics as a core of sacrificial cladding panels.

2.7.2. Knowledge gaps and thesis aims

So far, and up to the author's knowledge with the help of the reviewed literature, there is a lack on the assessment of the deformation behavior of sandwiched panels subjected to localized axial blast loads. In addition, tapered tubes were hardly found as the core of a sacrificial panel. Also, octagonal tubes received less attention than other conventional cross-sections, despite its excellent energy absorbing characteristics. That been said, all the aforementioned deficiencies listed, a system combining all of these modifications will respond differently to other geometrical configurations. The aim of this thesis revolves around the development of a sacrificial panel originally proposed by Theobald and Nurick [34]. This work added suggested developments to the sacrificial panel, such as the octagonal tapered tubes as core, that work on resisting the off-axis deformation of localized (hence, oblique) axial impulsive loading. For the sake of fully assessing the deformation behavior and the energy absorption characteristics of the panels, a geometrical study utilizing various influential parameters will be conducted. As will be shown in the methodology's chapter, the number of variables concerning the geometries is big enough, with much testing, to cover the intended study purpose. Therefore, finite element analysis acted as a perfect solution to reduce the needed resources, including time, to fully run the study.

CHAPTER 3. METHODOLOGY

3.1. Introduction

The explanation provided in this chapter will clarify the methodology followed in this thesis. Finite element analysis was the main solution and analysis method used to run the simulations for panels' performance analysis. The finite element model proposed is based on a previous published work by Theobald and Nurick [109], where they had already validated their work against experimental test data. On this thesis, a set number of influential geometrical parameters were varied over a range of values for the full analysis of the panel's response. In addition, the number of simulations needed to validate the response of the panel under these variables were using a design of experiment method. Therefore, the following sections will shed light on the FEM tool, components of the finite element model adopted in this thesis, and its validation.

3.2. Development of the FE model for octagonal core tubes of sacrificial cladding structures

3.2.1. FE tool

Finite element tools were built for many purposes, such as, analyzing the flow of fluids, structural mechanics, and many others. As this thesis studies the deformation behavior and energy absorption performance of structures, tools responsible for structural mechanics are the only ones of concern. Moreover, it should be noted that static and dynamic analysis are treated differently when it comes to the problem's solution algorithm. Static simulations deal with structures reaching an equilibrium state, that is, the long-time response under applied load. Whereas, structures subjected to

small durations of applied load or subjected to dynamic loads, then, dynamic simulations are the proper methods to dealing with them. Furthermore, finite element methods deal with elements, which are the fundamental components and the building blocks of a model, by finding the state of these elements after applying the specified load on them.

Newton's second law of motion $\sum F = ma$ is the basis of the finite element methods code for both of the static and the dynamic analysis. For both simulation types, the terms in the equation of motion comprises the internal forces in the structure (I) and the external applied forces on the structure (P), and, by forces the author refers to each element in the model. Moreover, inertial forces $M\ddot{u}$ are a distinct inclusion in applications of dynamic simulations, where M = mass of the structure; $\ddot{u}$ = acceleration of the structure, as shown in Equation 28.

Equation 28

$$M\ddot{u} + I - P = 0$$

A categorization of the load types considered in the Abaqus software and their solution algorithm is going to be fully addressed, until finally arriving at the package used in this thesis. Aside from the static-dynamic differences, dynamic simulations' solution code is dependent on another factor, which is the degree of linearity–and–non-linearity of the analyzed model. That mentioned, there are three linearity levels of dynamic problems in the Abaqus software: linear dynamic problems, non-linear dynamic, and explicit dynamic problems. The solution of linear and non-linear dynamic problems is provided by the implicit package of Abaqus. Implicit methods are defined by solving a system of equations in an iterative manner for each increment, until a small error criterion is met. On the other hand, the solution of explicit dynamic analysis is provided by the explicit package of Abaqus. Explicit methods solve by advancing the

kinematic state of the element through time from the previous increment, until the final time destination is reached.

Further on the subject, differentiating between linear and non-linear analysis is decided upon the problem type and the numerical model in hand. The sources of non-linearity are three: material, boundary and geometric non-linearities. In comparison with the study held in this thesis work, material non-linearity concerns the permanent plastic behavior of the structure. Boundary non-linearities concerns the contact conditions between the upper plate and the tubes, and the contact between the formed folds of the crushed tubes. While, geometric non-linearities concerns the large deflections underwent by the buckled tubes. With all these non-linearities present, and the significantly short duration of load appliance in shock events, it is decided that explicit analysis is the proper solution method for this thesis work.

3.2.2. Geometrical model and design of experiment

With the reasoning carried in Section 2.7.1, this section will list down the geometrical modifications to the chosen structures and their values range. The proposed sandwich panels consist of a top plate, core tubes, and a back plate. As aforementioned in the literature review, sandwich structures possess the fundamental characteristics of energy absorbers (Section 2.4.1). Regarding Stable deformation, sandwich structures are expected to possess such a characteristic, because of a load distributing top-plate and tapered-profiled thin-walled core tubes that work on preventing any out-off plane deformation resulting from load obliqueness. A number of potential-possessing design variables were chosen based of previously published work and those are the top plate thickness, cross-sectional ratio, tube thickness, taper angle, and the tube aspect ratio. The design variables, their symbols and values range are shown in Table 5. The

published work concerning the values of the top-plate and tube thicknesses, taper angle, aspect ratio, and, cross-section ratio were displayed in [61], [45], [34], and, [89], respectively. Mass allocation was applied to the octagonal tubes with different taper angle and cross-sectional ratio, to assure a fair comparison in assessment parameters. Taperness was considered from the mid-height of the tube, resulting in the mid-top portion of the tube decreasing in mass by a specific value, then the mid-bottom portion would increase by the same value, as compared to straight tubes (Figure 11). As for the cross-sectional ratio, the perimeter was fixed for both values, resulting in mass fixation (Figure 12).

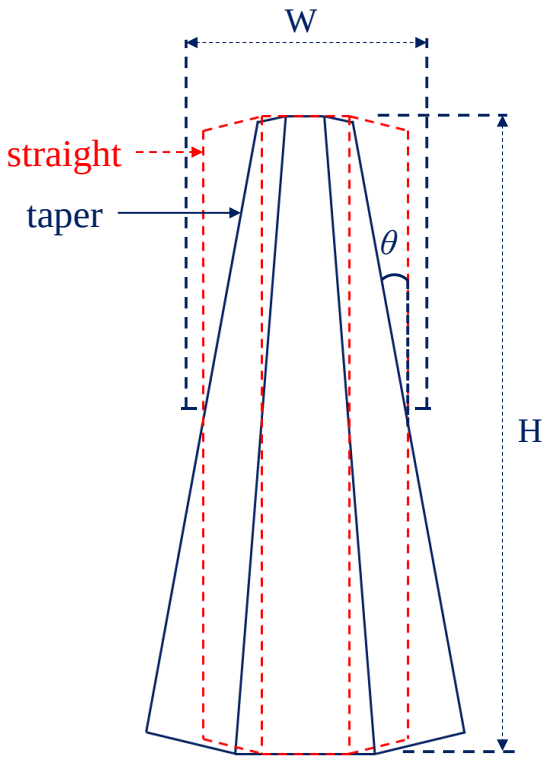

Figure 11. Straight-tapered tubes superimposition

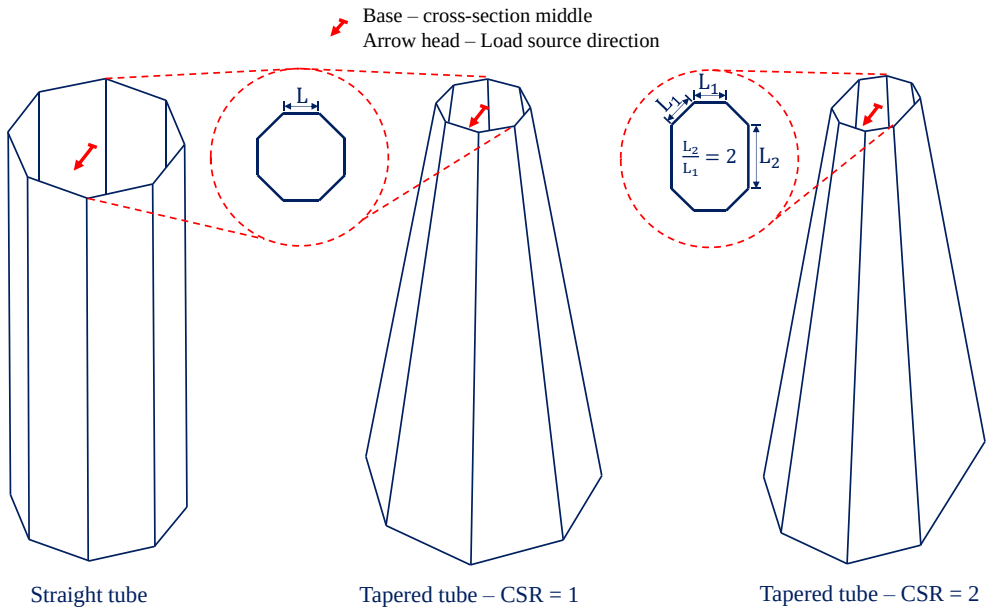

Figure 12. Core tube design concepts

Four tubes were considered in the panel core, and each tube had a length of 75 mm, the top-plate area was set at $150\ \text{mm} \times 150\ \text{mm}$. To ensure the stability of tube buckling, the tubes were positioned within the panel according to an essential parameter $\lambda = \frac{\lambda_1}{\lambda_2}$. λ represents the ratio of the distance from the panel center and the axis of the tube, to the distance from the panel center and corner of the top plate as shown in Figure 13. The optimum value of this parameter was found to be 0.528 as it gave the highest stability for the tube buckling of four core-tubes panel [34]. The core tubes were tied to the top and the rigid fully-fixed bottom plates via the 'tie constraint' with a contact algorithm of 0.3 friction coefficient. Finally, as this study considers multiple design variables, a number notation was given for each panel's configuration of the form "TPT – CSR – t – θ – R", where each of these parameters is listed in Table 5. As shown from the previous table, top plate and tube thickness, and cross-sectional ratio have two variables, additionally, taper angle and aspect ratio have three variables. Thus, this thesis should had been studying the work of 72 simulations in total. Unfortunately, all

tubes comprising a taper angle = 10° and an aspect ratio = 5 governed a very small tube top face. registered cumbersome for simulations, therefore, 8 simulations were reduced from the total number, concluding with a total number of 64 simulations. Moreover, Since the panel is symmetrical, only a quarter-symmetry of the full panel geometry was considered (Figure 14) to reduce the computational cost.

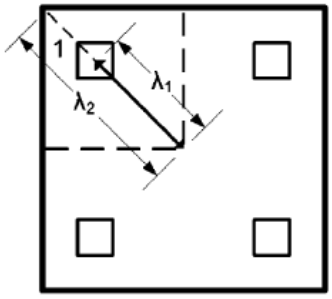

Figure 13. Top-view of panel design concept [2]

Table 5. Panel Geometrical Parameters

Design variable	**Symbol**	**Values**		
Top-plate thickness	TPT	2 mm		4 mm
Cross-sectional ratio	CSR	1		2
Tube thickness	t	0.6 mm		1.2 mm
Taper angle	θ	0°	5°	10°
Aspect ratio	R	3	4	5

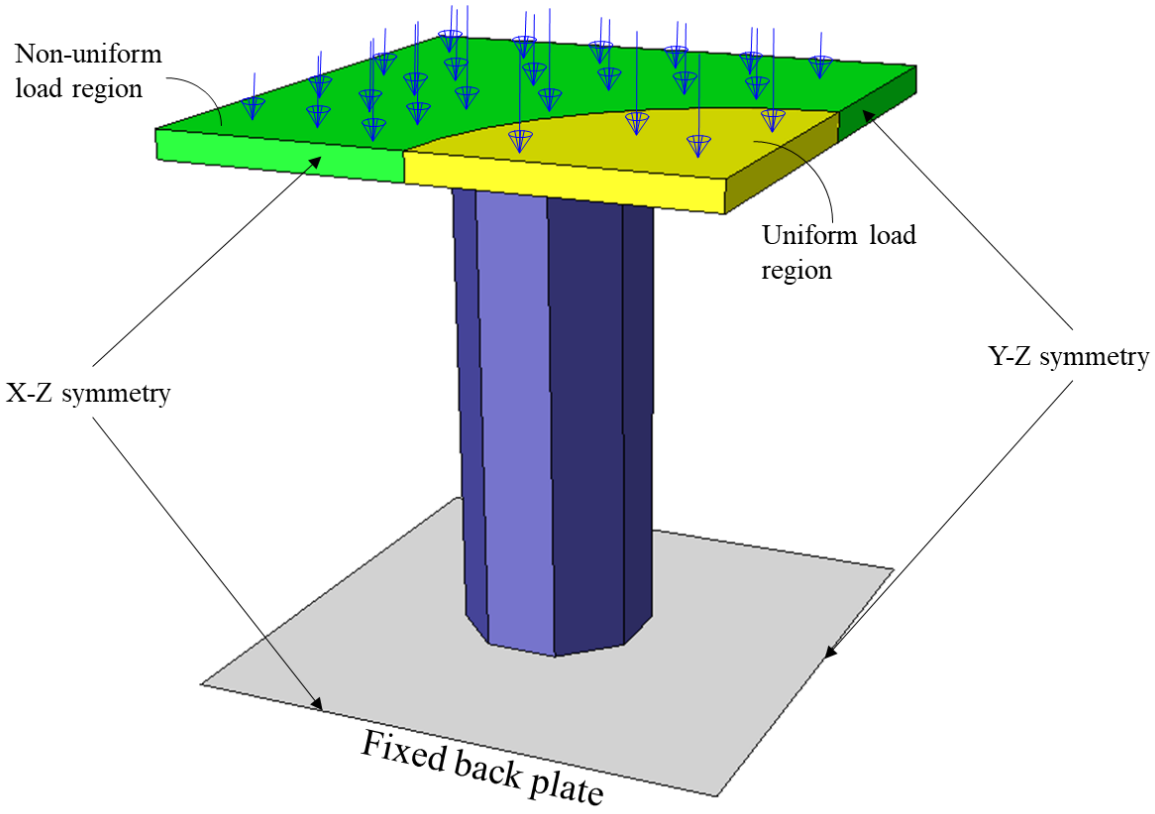

Figure 14. Quarter-symmetry of the numerical model's boundary and load conditions

3.2.3. Element type selection

Abaqus generally uses two types of blocks that are used for the calculation of the response in analysis: finite elements (i.e. deformable bodies) and rigid bodies. As obvious from the names, finite elements are deformable, hence, go through many degrees of freedom depending on the analysis in hand. On the other hand, rigid bodies are merely defined by six degrees of freedom, due to the undeforming behavior gone by the bodies. As expensive computational calculations are required to define the movement of the deformable elements, rigid bodies are considered much cheaper from a computational cost point of view. As this thesis focuses on explicit (dynamic) analysis only, it is worth mentioning that Abaqus/Explicit holds a subset of the elements

available in Abaqus/Standard where all elements types are available.

First, it is essential to mention that there are a large number of elements sets in Abaqus package (including rigid elements), and the availability of this set is essential as some problems could be solved by certain types, and the efficiency of the different elements varies with the problem statement. To easily distinguish between the different element types, five characteristics are considered: family, degree of freedom, number of nodes, formulation, and integration. A naming convection is assigned to the elements, stating the five characteristics, producing a unique name for each element. Simply stated, the first letter of the naming refers to the element's family, *C* = continuum elements, *S* = shell elements, and *R* = rigid elements. Degrees of freedom already differentiated for rigid elements. Furthermore, related to the family, some elements could have a feature of calculating the temperature effect, while others could calculate electric potential. In the same family, elements could have different number of nodes; an increasing number of nodes account for a higher accuracy, but, a longer computational time. Formulation refers to the mathematical theory used to define the element's behavior, and, element integration is set between the fully-integrated and the reduced-integrated schemes, which is going to be further emphasized later-on in this section.

The continuum, shell and rigid elements are the three element types that were used in the work of this thesis. Firstly, the continuum element type is the most capable of solving the widest range of simulation problems. While there exists a wide variety of the continuum family, but, it is recommended to rely on fully integrated elements: first-order (i.e. linear) hexahedral elements, or second-order tetrahedral which are a solution to complex shapes. These elements perform perfectly in the event of direct or shear loads, however, high bending strains result in a severe problem to fully integrated

elements, referred to as *shear locking*. For illustration Figure 15 shows a fully integrated first-order element subjected to bending moments, which give rise to shear stresses rather than the true bending deformation (Figure 16).

Figure 15. Deformation of 2D linear element with full integration under bending moment *M* [110]

Figure 16. Ideal deformation of material under bending moment *M* [110]

To overcome the issue of shear locking, high mesh refinement of second-order elements could serve as a practical solution, whereas a more practical solution is using reduced-integrated elements instead of fully-integrated ones. Reduced-integration elements use one fewer Gaussian integration point in each direction than the first-order elements (Figure 17), hence, are generally cheaper than fully integrated elements. Although linear reduced elements are less expensive and overcome the issue of *shear locking*, but, their drawback is the arise of what is referred to as the *hourglassing* or the zero-energy mode of deformation as shown in Figure 18. This deformation behavior is a result of the overly flexible properties of the element, which tend to be vulnerable to

the loads applied on it, being unable to resist with true-physics deformations. Because of the fault results introduced in linear reduced elements, an artificial *hourglassing stiffness* solution is introduced in the elements at the Abaqus software. Its general idea is to allow the elements to absorb the energy from the system and transfer it to the reduced elements, to let them react properly to the applied loads. The availability of the artificial stiffness in the elements is more efficiently performed when the simulated geometrical model is meshed with fine elements. It was recommended that for structures subjected to large bending strains, then, at least four linear reduced type elements to be used in the thickness of the model [110].

Figure 17. Position of integration points of 2D elements with reduced integration [110]

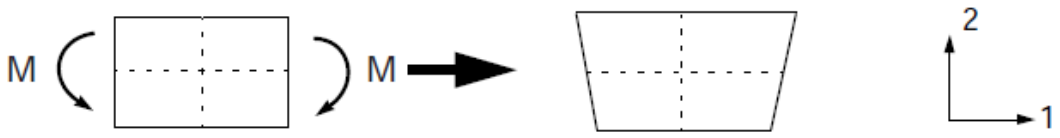

Figure 18. Deformation of 2D linear element with reduced integration under bending moment *M* [110]

On the other hand, shell elements serve as a more efficient element type in structures where one dimension, usually the thickness, is significantly smaller than the other dimensions, therefore, the stresses across the thickness are assumed negligible. Shell elements in contrast to 3D continuum elements are planar in geometrical discretization, but, are given integration points that extrude outside the plain in association with the thickness property assigned to the element. Shell elements acquire an interesting ability of either calculating the stiffness at the beginning of the analysis or during it. An elastic-plastic shell undergoing severe deformations might yield at the surface of the element (i.e. outer section point), while still possessing elastic behavior at the inner placed section points. Therefore, calculating the stiffness during analysis is more convincing in this thesis's work. Structures of isotropic material properties could be assigned five integration points which are adequate for most nonlinear models. The quadrilateral linear reduced-integration shell elements, similar in concept to the reduced-integration first-order continuum elements (Figure 19), are suitable for a wide range of applications.

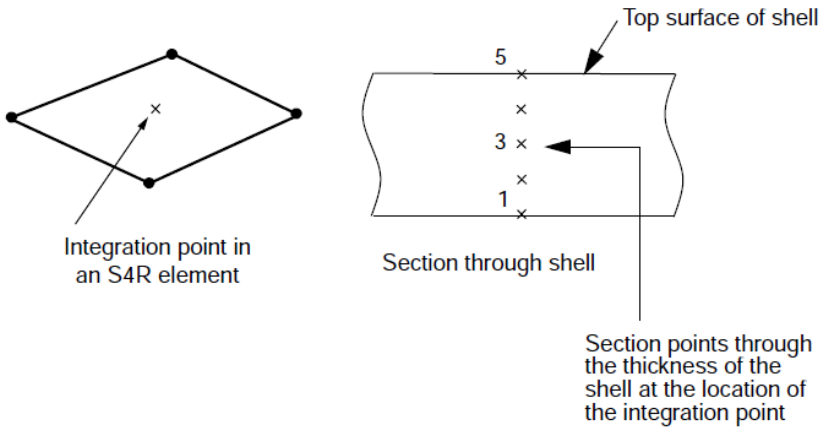

Figure 19. Configuration of section points across thickness of 2D integrated shell elements [110]

By compiling enough knowledge of the elements' categories, it is now time to decide on the elements selected for this thesis' analysis. As the study held uses a uniform cuboid shaped top plate, then the use of *C3D8R* element type (8-node reduced continuum elements) would be the best choice, from a behavioral and a computational cost point of view. Furthermore, the core tubes were modeled using *S4R* element type (4-nodes reduced shell elements) with five integration points across the thickness using gauss integration rule. Finally, with the design of a sacrificial structure, it is anticipated to model a bottom plate as a rigid body. Therefore, with the limited number of choices regarding the rigid elements, the bottom-plate was modeled using the R3D4 element type (the three dimensional 4-node rigid elements). It is worth mentioning that rigid elements collect all stresses applied to them at a single point which defines the whole rigid structure (i.e. the complete set of the rigid elements), namely, the reference point.

3.2.4. Boundary conditions

While the boundary conditions where explained in detail in Section 2.2.3, it is worth restating the load-distribution piecewise expressions and the initial load equations that are to be used in the simulations. The appliance of the load-distribution profile on the top face of the top plate of a sacrificial panel was adopted from the outstanding work of Theobald and Nurick [61]. Since impulsive loading was adopted, the pressure was adequately assumed to be a function of the spatial distribution only, $P(r,t) = P_s(r)$; as a matter of the time-pressure distribution playing a less significant role. The pressure distribution covered a circular region centered at the top plate with a high intensity, and exponentially decaying as moving radially outward toward the edges of the plate; in polar coordinates convention, the pressure distribution on the top-plate is defined as:

Equation 29

$$P_s(r) = \begin{cases} P_0^+, & 0 \le r \le R_0, \\ P_0^+ e^{-m(r-R_0)}, & r > R_0, \end{cases}$$

The value of P_0^+ was evaluated in terms of the positive impulse (I) applied on the panels as:

Equation 30

$$P_0^+ = \frac{I}{t_0^+ . [\pi . a^2 + 8 \int_0^{\pi/4} \left\{ \frac{-e^{\frac{m(-w+a\cos\theta)}{\cos\theta}} . (mw - \cos\theta) + (1 + ma) . \cos\theta}{m^2 . \cos\theta} \right\} d\theta]}$$

where $w =$ the half width of the top plate, with a prescribed value of 75 mm. Table 6 shows all parameter values needed to define the load on the panel. Also, a spatial distribution of the load is shown for the quarter dimension of the top plate in Figure 20, merely illustrating the distribution profile. It is important to mention that the blast duration value used is an estimate of the true value, however, it was claimed from the author that a small difference in duration for a fixed impulse causes insignificant effects on the panel's response [61].

Table 6. Pressure Distribution Parameters

I (Ns)	a (mm)	m (m^{-1})	t_0 (μs)
50	40	40	10

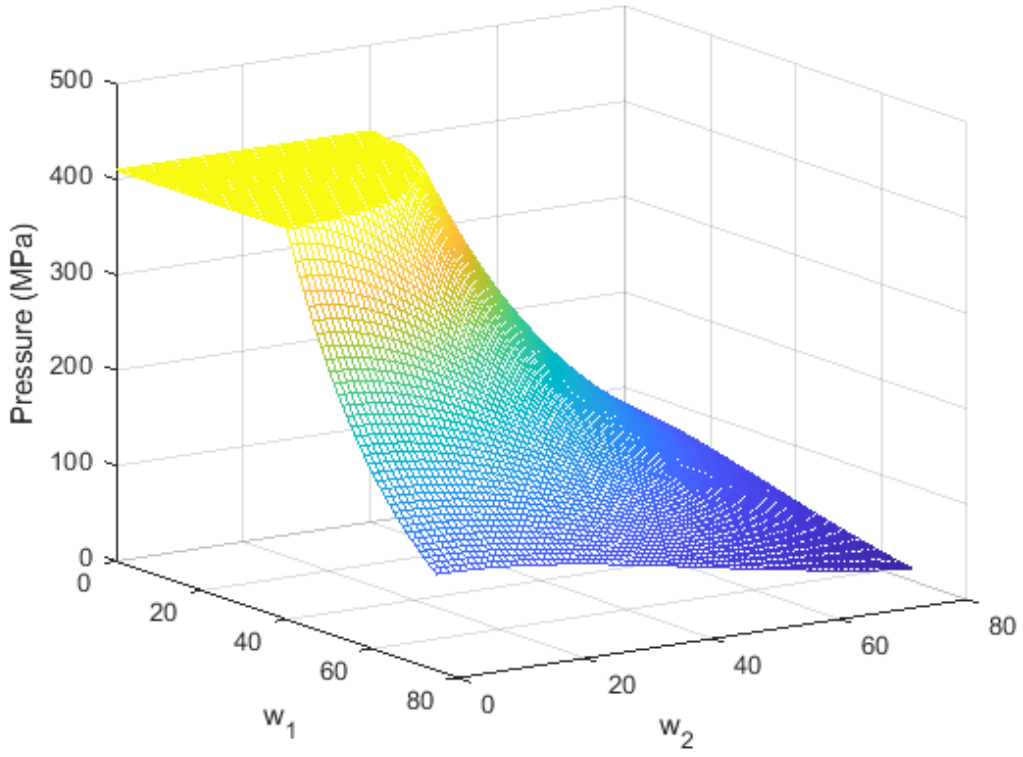

Figure 20. Blast load distribution across the panel's top-plate

3.2.5. Material model

The material employed to the top-plate and the tubes of the sacrificial panel is mild steel. Mild steel shows promising high strain-rate sensitivity compared to other types of metals such as aluminum, and less cost compared to composites. The true stress-strain values employed for the material model in the FE package are shown in Table 7, while the rest of the mechanical properties are listed in Table 8. The strain-rate effect was accounted for using the Cowper-Symonds model that formulates the ratio of dynamic to static flow stress:

Equation 31

$$\frac{\sigma_d}{\sigma_s} = 1 + \left(\frac{\dot{\varepsilon}_{pl}}{D}\right)^{\frac{1}{q}}$$

where σ_d, σ_s and $\dot{\varepsilon}_{pl}$ are the dynamic yield stress, static yield stress, and the plastic

strain-rate, respectively. While, D and q are Cowper-Symonds material constants, obtained from a set of tests conducted on a material's specimen of choice over a wide range of strain-rates, the points are then fit by the regression method.

Table 7. True Stress-True Plastic Strain of Mild Steel [61]

σ_0 (MPa)	223	224.81	229.50	237.08	246.11	254.06	259.83	264.89	268.50	272.83
ε_p	0	0.020	0.042	0.063	0.088	0.118	0.148	0.174	0.199	0.226

Table 8. Numerical Material Model of Mild Steel [61]

Density (kg/m^3)	Young's modulus (GPa)	Poisson's ratio	σ_0 (MPa)	D (s^{-1})	q
7850	200	0.3	287	2731	3.419

3.2.6. Mesh sensitivity study

Prior to running the parametric study, a convergence of the results with respect to the mesh size used in the model is to be attempted to assure the consistency of the results obtained. This procedure is called the mesh sensitivity analysis. The mesh sensitivity study aims to obtain consistent results with the maximum possible mesh size in the model, as any reduction in the mesh size has a significant increase in the computational run time of the studied model. Emphasizing on three main geometrical components in the studied model: the top plate, bottom plate, and the core tubes. So forth, for each component this analysis was based on the response parameters of the peak force (PF) and the energy absorption (EA), and the average maximum displacement attained by the tubes (δ).

Moreover, the meshes were varied as the size of the element for each of the top

and the bottom plates, and number of elements along the length of the core tubes. The values of the maximum displacement, energy absorption and peak force with the number of elements along the length of the core tubes, and the global size of elements of the bottom and the top plates are going to be illustrated in this section. The relative error percentages corresponding to each two sequential values of the assessment parameters are also displayed to show the converging scenario with the decrementing mesh size. Table 9 and Figure 21 demonstrates no affect with the increasing number of elements along the tapered tubes starting from 180 elements, therefore, the optimum condition in regard to the converging values of the assessing parameters and the least computational time is chosen, hence, 190 elements. Furthermore, Table 10 and Figure 22 shows the same procedure as that of the previous table, and a similar conclusion is withdrawn with the global size of 1 mm was chosen for the bottom plate, hence, the least number of elements on the bottom plate among the other choices. Finally, despite in the top plate (Table 11 and Figure 23) the decrementing global size of 1 mm to 0.9 mm showed negligible effect, but, the 0.8 mm size resulted in a relative error of 11% relative to 0.9 mm size. Moreover, although 11% is relatively noticeable, but, adopting 0.8 mm resulted in a much higher computation time to run a single simulation as shown in Table 12; computational time being a huge constraint to running 64 simulations in total, therefore, 1 mm of elements was chosen for the top plate elements.

Table 9. Core Tubes Element Size Optimization

Mesh average edge length (mm)	**180**	**190**	**200**	**210**
Maximum displacement (mm)	45.12	44.73	45.22	44.73
• Relative error (%)	-	0.87	1.10	1.07
Energy absorption (kJ)	399.47	399.52	399.12	399.30
• Relative error (%)	-	0.01	0.10	0.04
Peak force (kN)	84.84	84.94	85.03	85.15
• Relative error (%)	-	0.11	0.11	0.14

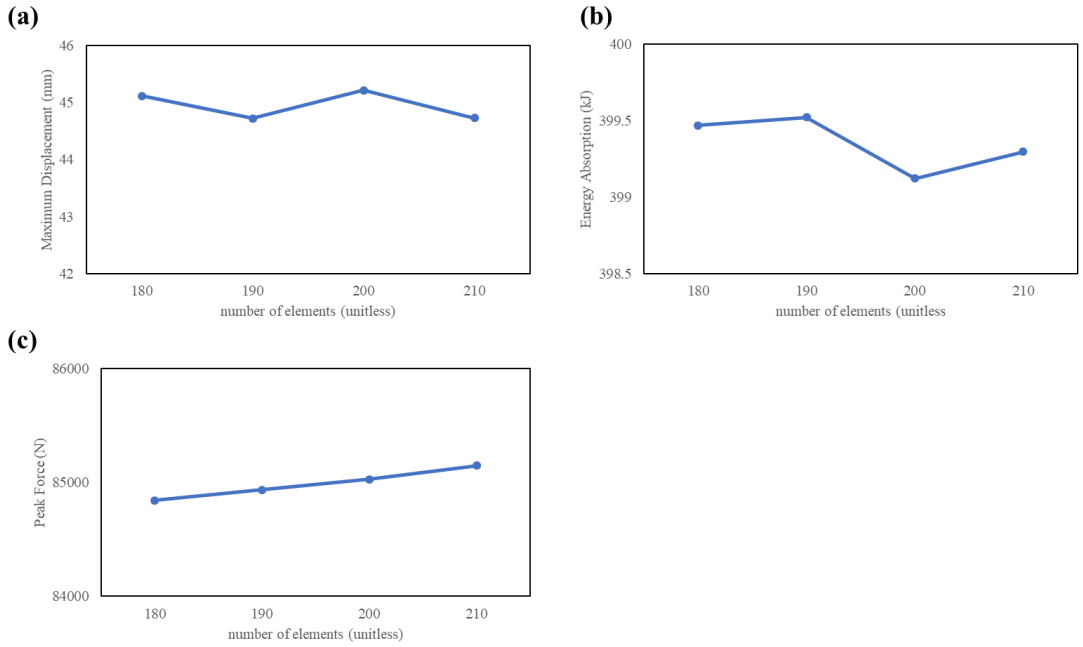

Figure 21. Mesh sensitivity analysis of the tubes

Table 10. Bottom Plate Element Size Optimization

Average element size (mm)	**1.0**	**0.9**	**0.8**
Maximum displacement (mm)	45.12	44.91	44.79
• Relative error (%)	-	0.47	0.26
Energy absorption (kJ)	399.47	399.08	399.03
• Relative error (%)	-	0.10	0.01
Peak force (kN)	84.84	84.84	84.86
• Relative error (%)	-	0.00	0.01

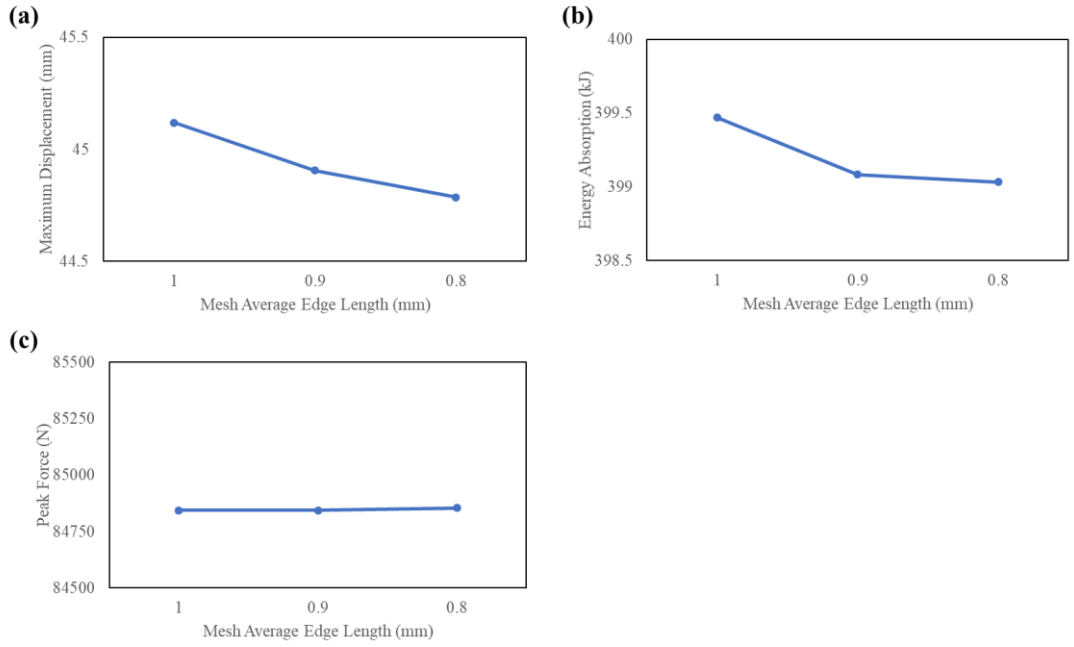

Figure 22. Mesh sensitivity analysis of the bottom plate

Table 11. Top Plate Element Size Optimization

Average element size (mm)	**1.0**	**0.9**	**0.8**
Maximum displacement (mm)	45.12	44.99	50.02
• Relative error (%)	-	0.27	11.16
Energy absorption (kJ)	399.47	398.54	396.65
• Relative error (%)	-	0.23	0.47
Peak force (kN)	84.84	84.55	79.96
• Relative error (%)	-	0.35	5.43

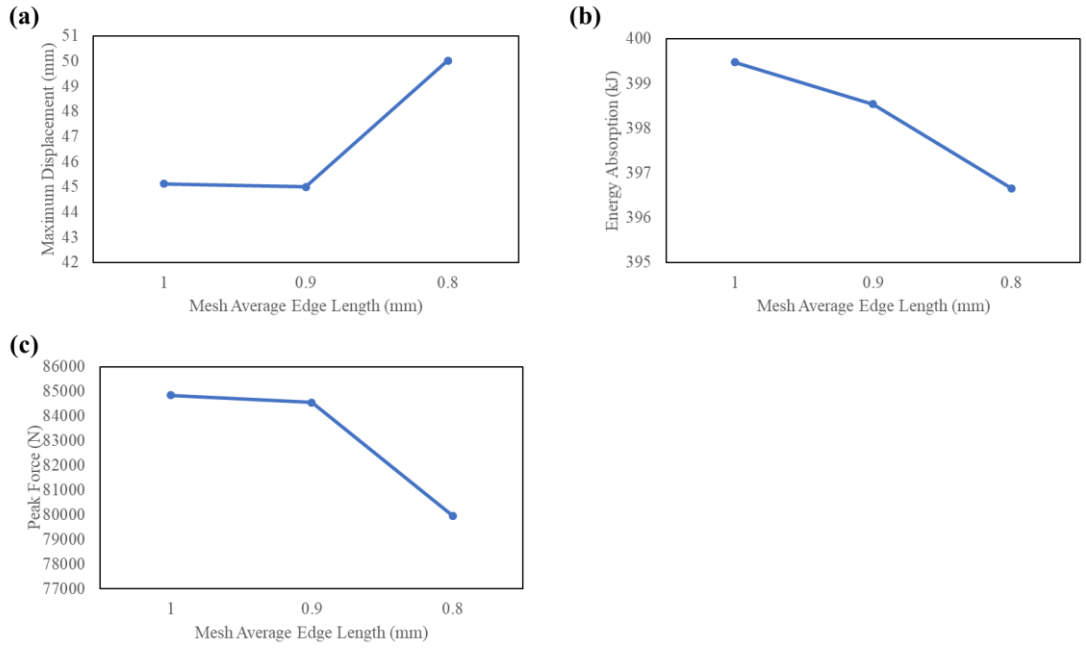

Figure 23. Mesh sensitivity analysis of the top plate

Table 12. Computational Time Dependence on the Average Size of the Top Plate's Elements

Average element size (mm)	1.0	0.9	0.8
Computational time (hrs:mins)	3:30	6:45	10:00

3.3. Validation of the FE model with experimental tests

The best validation technique of numerical models is by building the model upon experimental tests. Keeping in mind that this thesis is revolved around impulsive loads that come from explosive detonations, unfortunately, carrying experimental tests was impossible. This is due to the governmental restrictions and obstacles on detonating explosives by individuals or a testing team. Therefore, providing the needed equipment for testing was not possible. An alternative efficient solution to carrying the validation of the FE model, is by using a readily available model from previously published work. To ensure that the model is employed correctly, the model is reconstructed and validated from the experimental data published. The model reconstructed for validation is readily developed, it is composed of a nine mild steel core-tubes distributed evenly across the sacrificial panel (Figure 24), with a top-plate area of $150\ \text{mm} \times 150\ \text{mm}$ and 4 mm thickness. Each tube is 75 mm long and 0.61 mm thick, with a tube positioning λ of 0.70. The blast load had a uniform pressure distribution with a pressure value of 274 N/mm^2 and a pressure-time distribution of:

Equation 32

$$P(t) = \begin{cases} P_0 & 0 \le t \le t_0 \\ 0 & t > t_0 \end{cases}$$

Equation 32 implies a special case of Equation 29, where the *m* previously defined is zero. The blast duration t_0 was assumed to be $10\ \mu\text{s}$, as done in the published work, claiming that extending the duration period will not affect the response of the panel significantly.

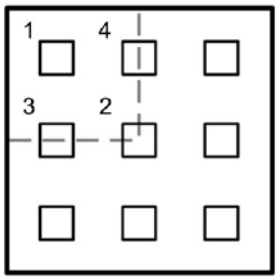

Figure 24. Nine core-tubes panel layouts [34]

The force-displacement diagram for a nine core-tubes panel from [61] is mapped and plotted against the force-displacement diagram obtained for the same panel using the developed finite element model as shown in Figure 25. It was observed that the course of progression of the force with displacement matches well with the published data. Furthermore, the peak force, crush distance, and energy absorbed were extracted and compared as listed in Table 13. It is worth mentioning that despite the compared models concerning the plotted graphs being both finite element models, but, some observed differences are there. One possible reason behind the plot progression difference in the unaccounted embedded thermal softening model of the applied material models. After reviewing, it was found that the thermal softening model had an insignificant effect on the overall panel performance, especially on the energy absorption. Therefore, it was not accounted for in this study to reduce the computational time [74]. Afterall, under these conditions the model is considered validated, hence, can be used to predict the response of sacrificial panels of octagonal core tubes under blast loading conditions.

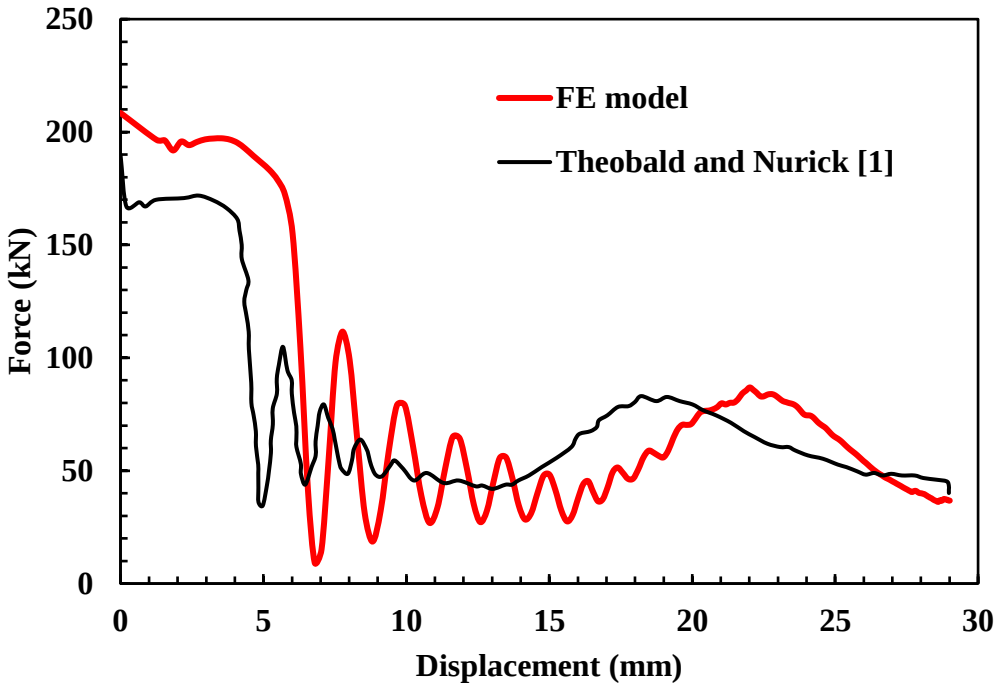

Figure 25. Force-displacement curve of current FE model and Theobald and Nurick [61], both for panels of 9 core tubes

Table 13. Finite element models assessment parameters' values difference

Reference	**PF (kN)**	***δ* (mm)**	**EA (kJ)**
Published data [61]	190	30	2.35
Current Study	208	29.44	2.32
Error (%)	9.5	1.86	1.29

3.4. Summary

This chapter presented the methodology followed prior to running the simulations, emphasizing on the methodology being based to high extent on the previous published work of Theobald and Nurick [109], where their work had been already been validated against experiments. Furthermore, this chapter had also shed

light on the FEM tool and on the separate components of the finite element model; detailed explanation and visualization of the geometrical models, summarized in the design of experiment section of this chapter. Moreover, an explanation over the different element types was demonstrated, finally, ending with every element of choice related to the geometrical component in the FE system. In details, the top plate adopted the *C3D8R* element type, R3D4 element types were chosen for the bottom plates, and finally, *S4R* element types were chosen to the tapered core tubes of the sandwich panels.

A brief explanation of the mathematical background of the boundary conditions was present to know the basis behind the development of the model. Furthermore, an illustration of the distribution of the load was present to give an idea on the load appliance at the top plate. The material model had also received care, keeping in mind that all structures of the finite element model had 'mild steel' as the material of choice. On top of that, strain-rate sensitivity of the material being highly crucial, the Cowper-Symonds model was the model of choice since this model is highly developed, and the constants of this model for 'mild steel' are highly reliable from literature. Furthermore, a mesh sensitivity study in terms of the maximum crush distance, peak force and energy absorption was conducted to assure the reliability of the results obtained from simulations. An optimum global size of 1 mm was assigned to the top-plate, tubes and the rigid bottom plate. 190 elements along the tube length was the optimized number of elements, taking convergence and computational costs into account. Finally, the same tools were used to build a similar model to that of the experimental tested system from Theobald and Nurick **[1]** to go through the steps of validation of the model in hand. The validation step gave confidence on using the results obtained from the built finite element models, rendering the models reliable.

CHAPTER 4. SACRIFICIAL CLADDING PANEL SUBJECTED TO NEAR-FIELD IMPULSIVE LOAD

4.1. Introduction

After completing all the required models, running the mesh sensitivity study on them, and validating them, it is time to run the simulations determined from the design of experiment. Also, this chapter focuses on analyzing the data acquired from the last technical step of this thesis. For instance, the assessment of the simulated panels is based on the force-displacement diagrams of the loaded panels, the buckling behavior of the tubes, and on each of the peak force, stroke efficiency, energy absorption and core efficiency. A summary briefing out the important analyzed results is given at the end of this chapter.

4.2. Force- and energy absorption-displacement characteristics

Figure 26 shows typical force-displacement and energy absorption-displacement diagrams for sacrificial panels of *TPT* of 4 mm, *CSR* of 1, t of 0.6 mm, *R* of 3, with varying θ. This was done to solely investigate the effect of the taper angle on the performance of the core tubes. From Figure 26–b, it is evident that increasing θ results in a higher post-buckling forces fluctuation, but, sustaining the force levels for higher stroke, hence, leading to a more stable deformation behavior. The increased fluctuations are a result of the bigger tube's cross-section encountered moving down the tube's length, adding a stiffer component to the tube. While the higher stability is caused by the tube taperness, which is more immune to oblique loading that facilitates off-axis buckling. Furthermore, the crush distance recorded an increase with increasing θ. This is due to the low resistance in tapered tubes that corresponds to the smaller top

diameter (subsequently moment of inertia) of the tapered tubes, which is a result of fixing the tube's mass with a varying taper angle.

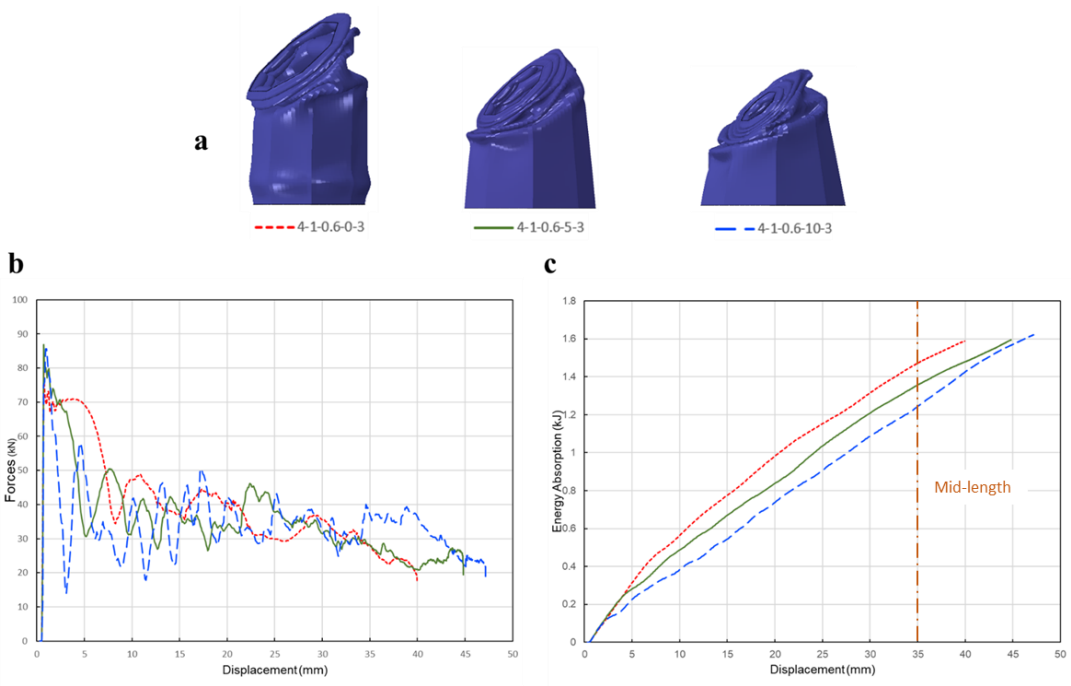

Figure 26. (a) Crushed tubes of panel 4-1-0.6-θ-3 with a varying taper angle (b) plot of force-displacement curves of the same crushed tubes; and (c) plot of energy absorption-displacement curves of the same crushed tubes

The energy absorption-displacement curves showed a decrease in the slope of energy absorption with the increase in θ as shown in Figure 26–c. Elaborating more, the energy absorption per unit length (EA/L) was higher for straight tubes ($\theta = 0$), up to the mid-length of the tube (δ = 35 mm). Due to the taper nature, tubes tended to sustain similar EA/L levels, while it dropped for straight tubes. Sustaining the EA/L levels for tapered tubes was attributed to the increasing mass moving down the tapered tube's length. Additionally, the higher crush distance was attributed to the gradually increasing moment of inertia of tubes of higher θ. In taper tubes' top section, the lower

moment of inertia allowed for a faster rate of crushing as compared to straight tubes. However, the diameter increase associated with crushing progression resulted in a slower crushing with time. The slow crushing allowed for more crushing time, hence, the tapered tubes had a higher overall crushing distance. It is worth mentioning that the effects of top plate and tube thicknesses were only restricted to the magnitudes of crushing forces and energy absorption. Finally, their effect with the other geometrical parameters will be discussed in detail in the following sections.

4.3. Buckling behavior

An important aspect to look at when analyzing a thin-walled tube under compression is the deformation mode. Various deformation modes of tubes imply different tube behaviors, folds shape, EA efficiency, and stability during buckling. The core tubes' deformation modes were categorized into four typical modes, utilizing different sets of top plate and tube thicknesses as shown in Figure 27. Mode 1 of deformation was the most progressive deformation mode, with mixed folds and a tilted tube top due to the oblique nature of loading. This is due to the effective pressure wave distribution with the help of the thick top plate. Mode 2 of deformation is the tube forming a single biased fold toward the load source. This behavior gave an insight of the overly thick tubes, thus, less flexibility to the deformed tubes. It was evident that the top- and bottom-plates contacting was majorly avoided in panels with a plate thickness of 4 mm (Figure 28).

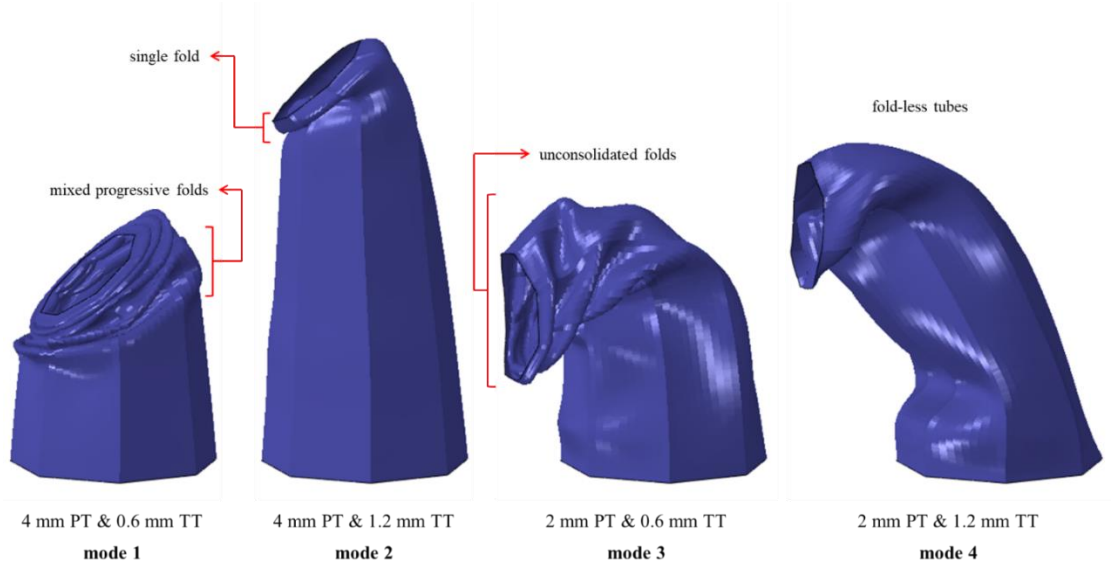

Figure 27. The four modes of deformation for tubes of CSR =1, θ = 5° and R = 3 and different TPT and t

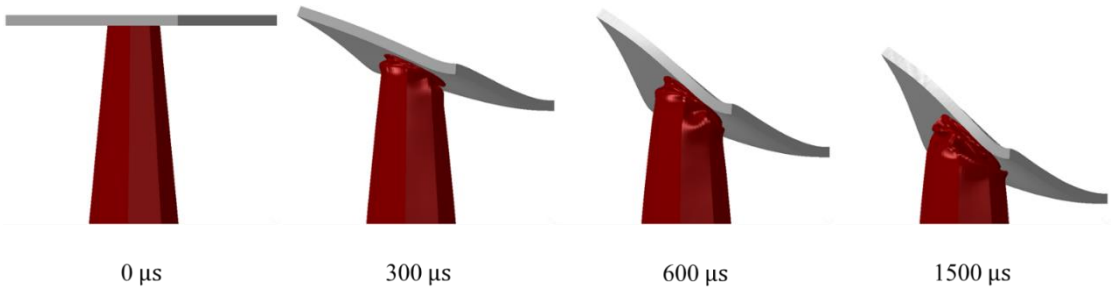

Figure 28. '4-1-0.6-5-3' panel deformation behavior with time

Tubes with Mode 3 experienced Euler buckling and formed a high number of folds, with most folds being biased and unconsolidated. This resulted from the high obliqueness associated with the overly thin top plates. Moreover, panels undergoing Mode 4 are the fold-less core tubes, with a middle flattening undergone by all tubes. Some cases in sets of plate thickness and tube thickness of Mode 4 registered fold-like bulges created beneath the proximal end, directed toward the load source (Figure 29). It is worth mentioning that all panels with a plate thickness of 2 mm underwent Euler buckling. An example of a panel in this set is shown in Figure 30.

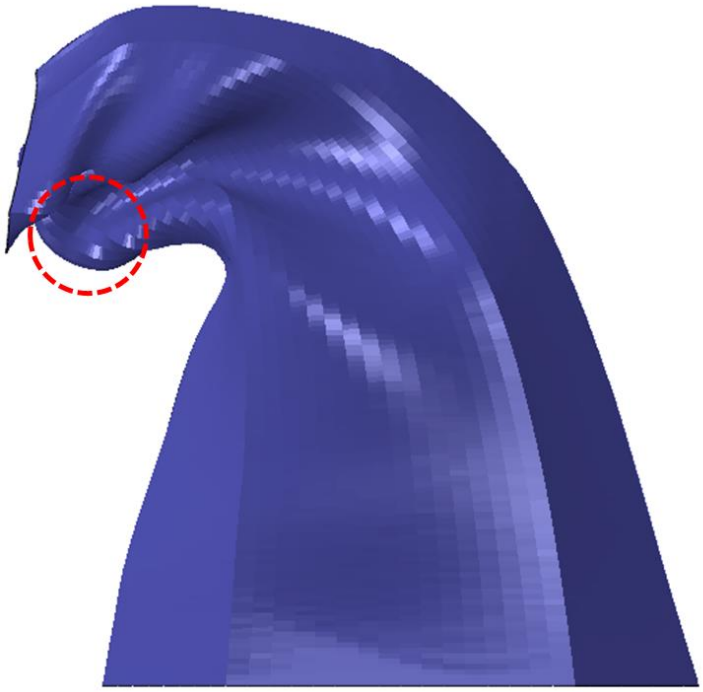

Figure 29. Fold-like bulge of core tube of panel '2-2-1.2-10-3'

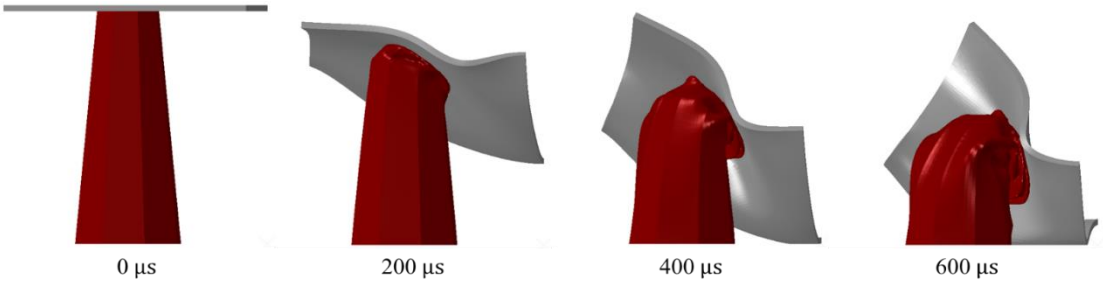

Figure 30. '2-1-0.6-5-3' panel deformation behavior with time

Moreover, tubes of cross-sectional ratios of 2 were able to form multiple global bending hinges compared to tubes of cross-sectional ratios of 1 (Figure 27). This resulted in the leading panels in terms of energy absorption to have cross-sectional ratios of 2. Finally, panels with a plate thickness of 4 mm and tube thickness of 1.2 mm had folds formed toward the load direction only, while biased folds were created in all panels with a plate thickness of 2 mm.

4.4. Influence of assessment parameters

The geometrical parameters and the sacrificial panels' responses are presented in the table in APPENDIX. A detailed analysis and explanation of the panels' response is presented in the following sections.

4.4.1. Influence on initial peak force (PF)

Figure 31 shows the average effect of the geometrical parameters on the peak force. As can be seen form the figure, there was an insignificant decrease in the peak force in thick top plates as compared to thin top plates. This decrease occurred because the thin plates are associated with a smaller inertia, hence, experienced higher attained velocity, therefore, strain hardening effect was taking part in the tube buckling. Furthermore, the aspect ratio is another parameter that influenced PF significantly with a negative correlation. This is attributed to the less resisting material against the load causing buckling. Similar behavior was reported in Theobald and Nurick [34] for straight tubes against blast loading. Conversely, PF was found to almost double in value when doubling the tube thickness (APPENDIX). This increase can be attributed to the stiffer thicker tubes, resulting in higher loads to initialize crushing.

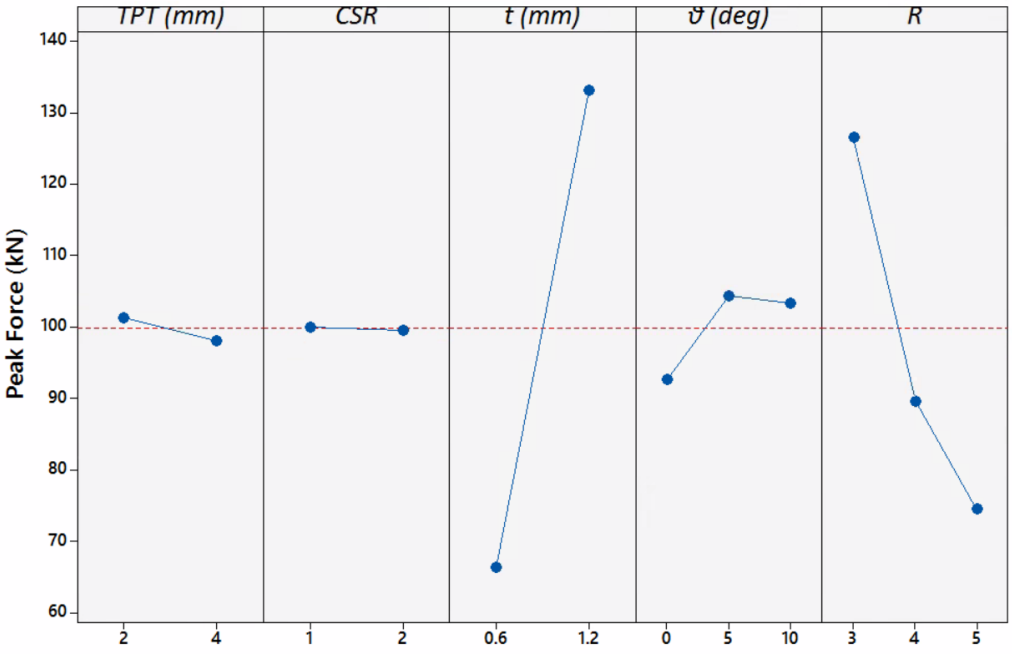

Figure 31. Influence of geometrical parameters on peak force

Likewise, the taper angle had an alternating influence on the peak force. Unconditionally, the peak forces were highest for all tubes with a taper angle of 5°. Whilst, PF was lower for a theta of 0° and 10°, with an absolute difference between them ranging from 1.46 kN – 15.12 kN (APPENDIX). The reason behind this alternating behavior of taper angle shows a compromise between the effect of inertia, strain and strain-rate hardening. Where tubes of a higher mass above mid-length acted stiffer to initiate buckling (i.e., lower taper angle), because of the higher inertia and the strain hardening effects. Simultaneously, these tubes experienced slower buckling, resulting in smaller strain-rate hardening effects. As an example, panels with a top-plate of 4 mm, cross-sectional ratio of 1, tube thickness of 0.6 mm and an aspect ratio of 4 had a PF of 57.24, 65.39 and 53.94 kN for a theta of 0°, 5°, and 10°, respectively. Finally, it was shown that the cross-sectional ratio was the only geometrical parameter that had no effect on the PF.

4.4.2. Influence on stroke efficiency (ε_{stroke})

Since the tubes' length was fixed, the average effect of the geometrical parameters on the stroke efficiency was plotted in Figure 32 instead of the crush distance. It can be seen from Figure 32 that a response similar to the peak force was observed for the tube's ε_{stroke} for a taper angle of 0° and 5°, however, the value increased for a 10° taper angle. This recalls the response of peak force in 5° taper, where the strain-rate hardening effect was higher than inertia effect, resulting in a higher resistance in the tubes, hence, less deformation. Moreover, aspect ratio was found to increase ε_{stroke} in a near-uniform manner. Moreover, it was deduced from the table in the APPENDIX that the increase of ε_{stroke} with aspect ratio was higher in panels with thicker top-plates than thinner ones, with an average increase of 0.06 and 0.02, respectively. This is attributed to the general change in deformation mode when changing from a top-plate of 4 mm to 2 mm as stated in Section 4.3.

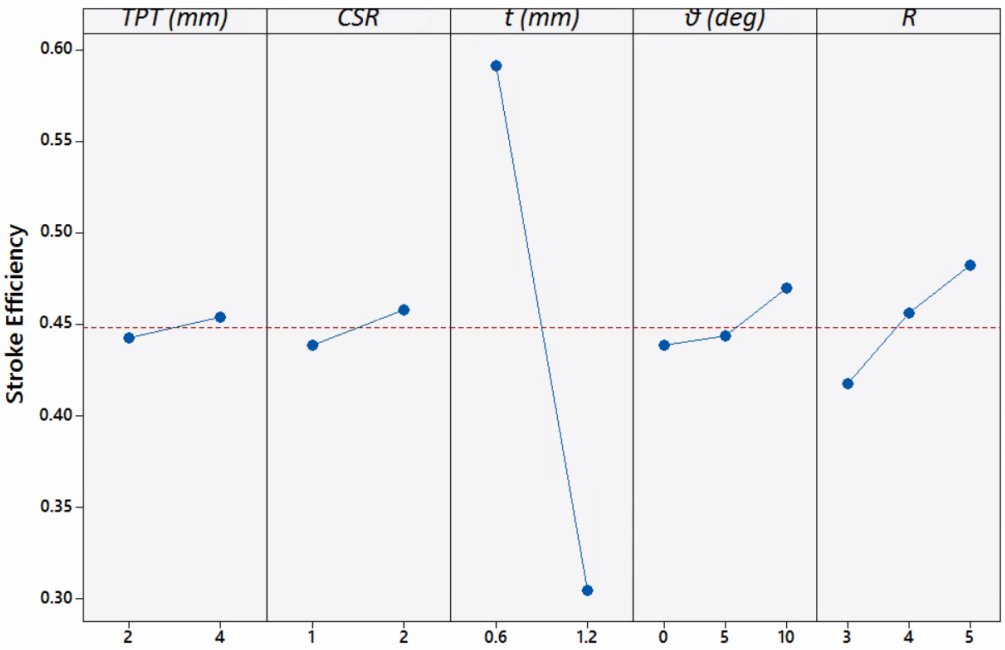

Figure 32. Influence of geometrical parameters on ε_{stroke}

Top-plate thickness and tube thickness developed an interaction influence on $\varepsilon_{\text{stroke}}$ (Figure 33). The value of $\varepsilon_{\text{stroke}}$ for a top-plate thickness of 4 mm and tube thickness of 0.6 mm was the highest with an average of 0.68, and the lowest value corresponded to a plate thickness of 4 mm and a tube thickness of 1.2 mm with an average of 0.23. Panels with a plate thickness of 2 mm forced the tubes to deform excessively until plates contact occurred, which resulted in high $\varepsilon_{\text{stroke}}$ values. Moreover, because of the sufficient load distribution of thick plates, thin tubes highly contributed to the crushing, deforming the furthest. This finding conforms with Theobald and Nurick [34] suggesting the use of thick plates for an idealized panel performance. Lastly, the cross-sectional ratio was found to cause a slight increase in $\varepsilon_{\text{stroke}}$. This could be a result of the narrower smallest width in tubes with a cross-sectional ratio of 2 compared to the other cases, rendering the tubes unstable.

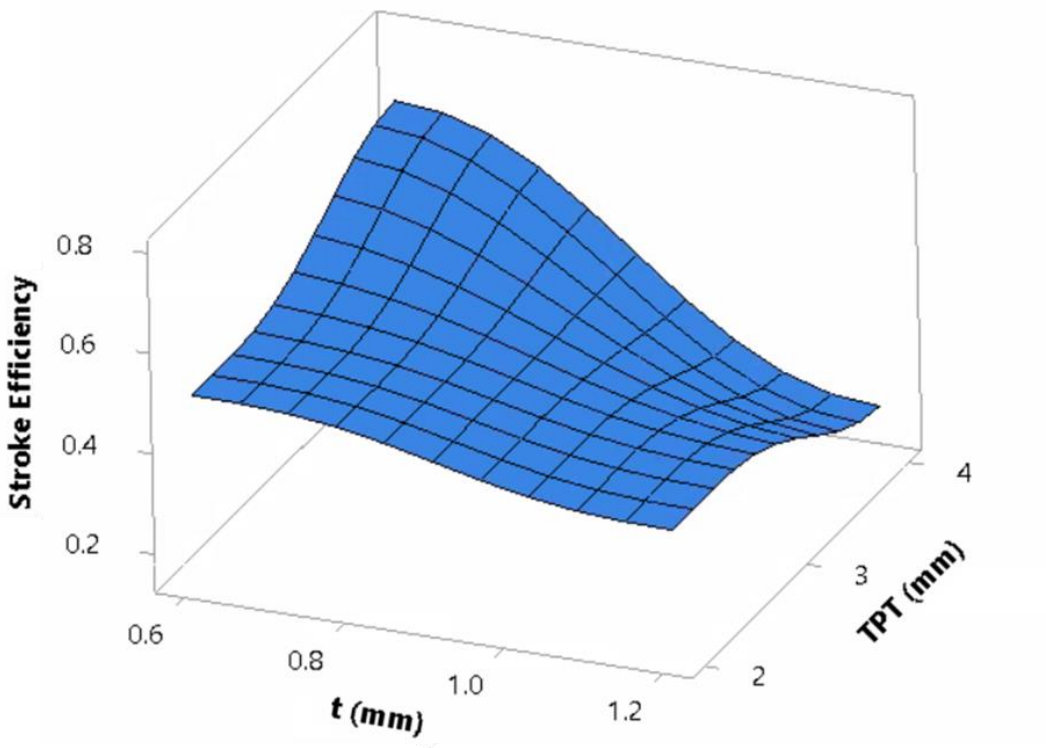

Figure 33. Dependence of ε_{stroke} on the interaction of top-plate and tube thicknesses

4.4.3. Influence on EA and ε_{core}

The average effect of geometrical parameters on EA is depicted in Figure 34. From the figure, energy absorption of the panels was highly influenced by the plate thickness, due to the deformation mode underwent by the different tube configurations. Because of its big significance on EA, it is worth investigating EA individually for thin and thick plates panels. Once plates-contact occurred in panels with thin tubes, EA decreased with the increase of taper angle and aspect ratio due to the corresponding stiffness decrease (APPENDIX). Opposingly, thick tubes increased EA in panels with taper angle and aspect ratio, although, Euler mode of buckling was dominating. Hence, panels with a plate thickness of 2 mm and a tube thickness of 1.2 mm had the highest EA value with the leading panel being '2-2-1.2-0-5', with a value of 2.34 kJ. This is because panels with a plate thickness of 2 mm forced thick tubes to crush similar to thin tubes, and due to the high stiffness of thick tubes, they tend to absorb higher energy than thinner ones.

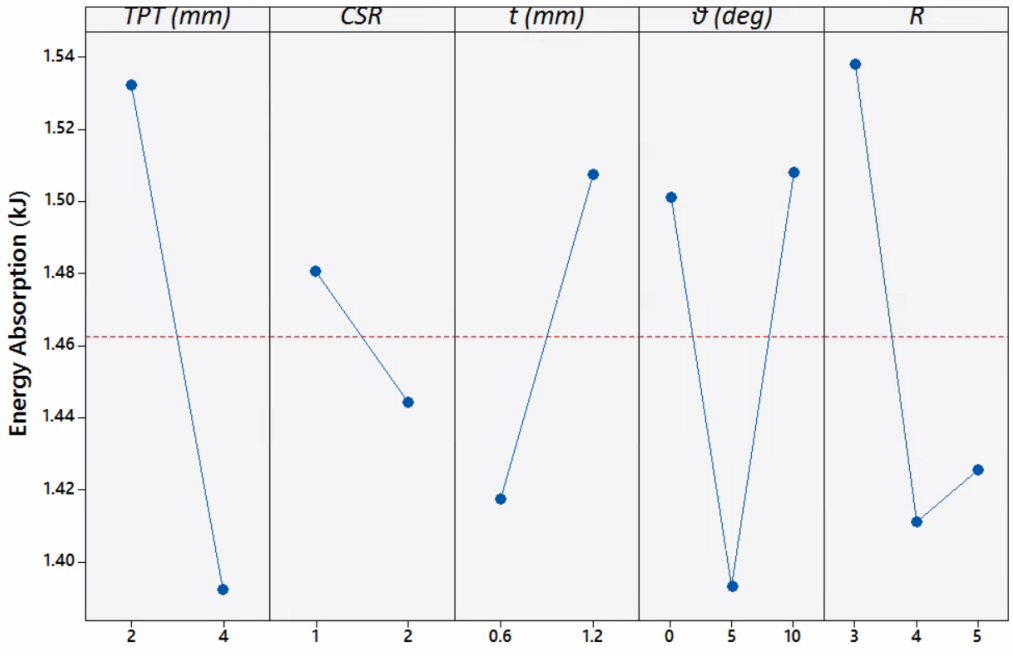

Figure 34. Influence of geometrical parameters on energy absorption

Moreover, tubes with a taper angle of 5° among others were found to absorb the least energy for a plate thickness of 2 mm and a tube thickness of 1.2 mm. This result highlights the unfavored effect a small taper holds on thin-walled energy absorbers under high strain-rate oblique loading. Furthermore, from a deformation point of view, tubes with a cross-sectional ratio of 2 formed lower number of rings relative to other tubes with a cross-sectional ratio of 1, resulting in a decrease in EA. In contrast, there were some cases that found cross-sectional ratio of 2 absorbing higher amounts of energy than tubes with a cross-sectional ratio of 1. Afterall, generally speaking, no trend was found relating energy absorption to the cross-sectional ratio. The interaction plot in Figure 35 between the top-plate and tube thicknesses summarizes the previously stated behavior of the panels in terms of EA, due to their high observed influence on EA. From here, it was observed in general that panels with a thin plate and a thick tube absorbed the most EA with an average of 1.79 kJ, and, panels with a thin plate and a thin tube absorb the least with an average of 1.27 kJ.

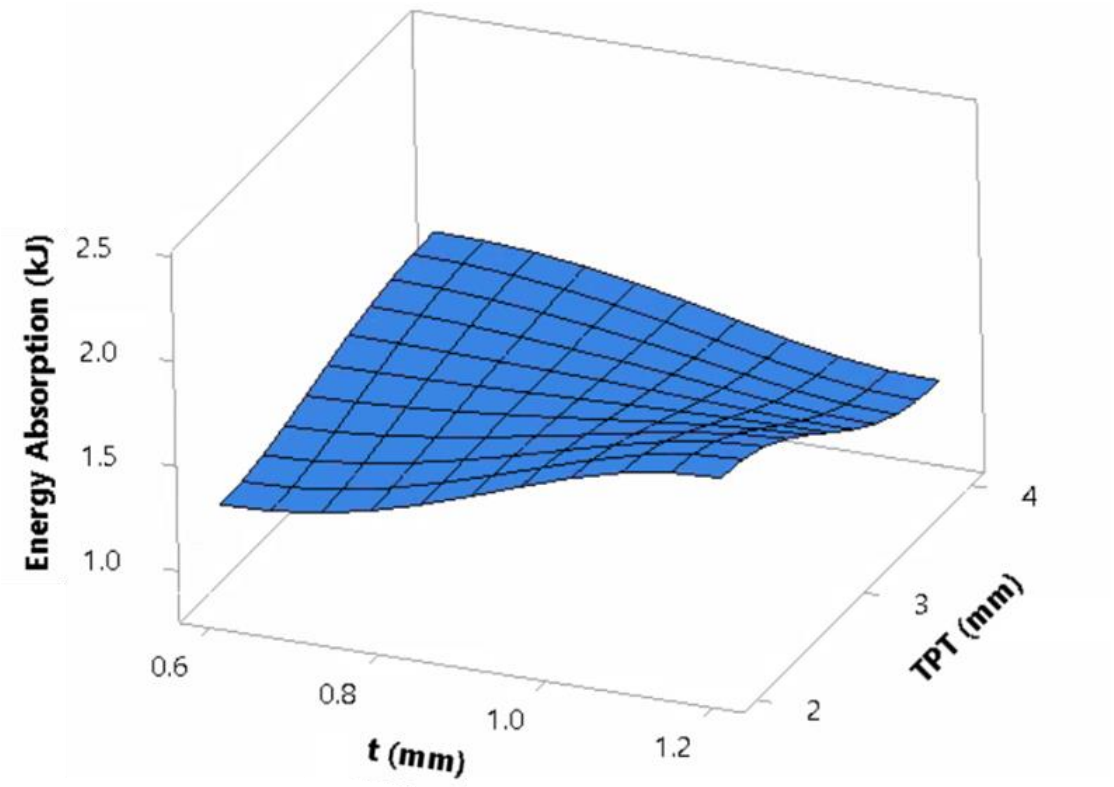

Figure 35. Dependence of energy absorption on the interaction of top-plate and tube thicknesses

To further understand the panels' behavior, the effect of geometrical parameters on core efficiency, ε_{core}, is depicted in Figure 36. ε_{core} is the ratio of energy absorbed by the core only to the work done on the whole panel. As shown, the influence of the top-plate and tube thickness on ε_{core} opposed the effect on that of EA, while, the influence of taper angle and aspect ratio were similar. To elaborate more, the interaction of the top plate and tube thicknesses is depicted in Figure 37. Unconditionally, thicker plates caused the panels to perform more efficiently than panels with thin plates in terms of ε_{core}, with a percentage increase of 73.5%. This is attributed to the higher level of buckling progression in thick plate's panels as compared to that of the thin plate's panels that suffers from Euler buckling. Similar findings were reported by researches assessing thin-walled tubes subjected to compression [91,111]. Another reason to the drastic fall

of ε_{core} in thinner plated panels is the contact between the top and back plates. The contact caused a very high amount of work applied on the non-sacrificial structure, despite the higher energies absorbed by the core, leading to a decrease in ε_{core}.

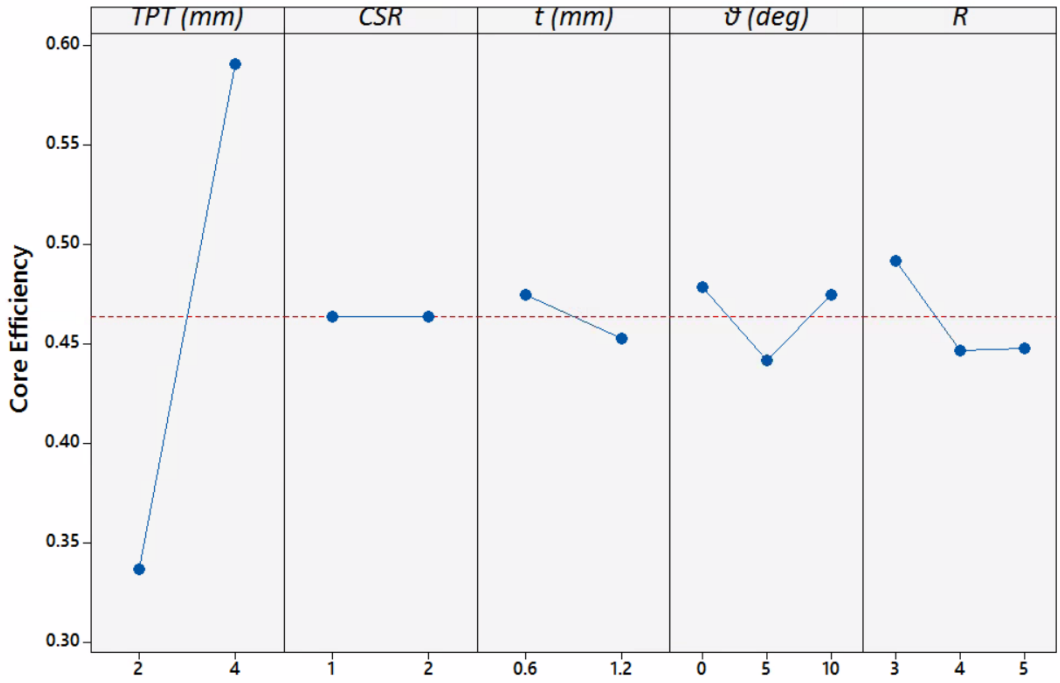

Figure 36. Influence of geometrical parameters on ε_{core}

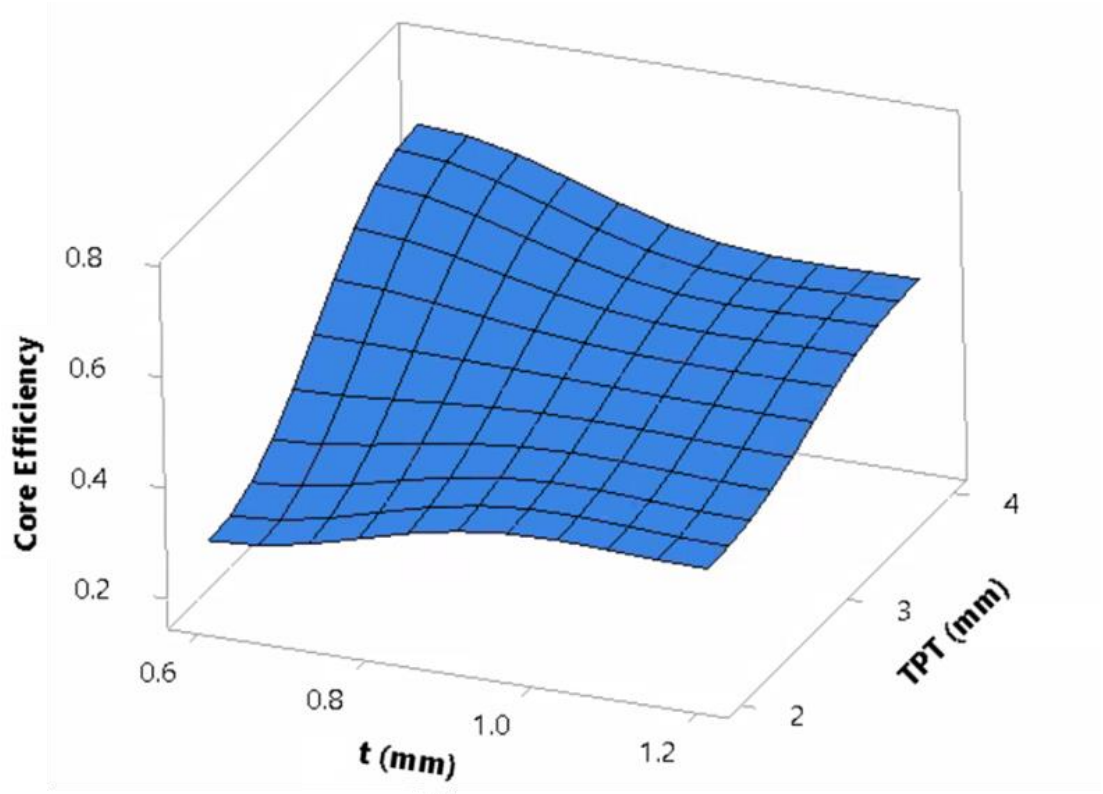

Figure 37. Dependence of ε_{core} on the interaction of top-plate and tube thicknesses

4.5. Summary

An investigation on the performance of sacrificial panels with straight and tapered core tubes of varying geometrical parameters of taper angle, aspect ratio, tube thickness and cross-sectional ratio, and thicknesses of the top plate was held in this chapter. While some geometrical parameters were found more influential than others from an energy absorption and a buckling behavior characteristic point of view, it is worth noting that the cross-sectional ratio was relatively of no influence on the panel's behavior. Furthermore, small taper angles of 5° exhibited unfavored absorbing and buckling characteristics, whereas, bigger taper tubes of 10° resulted in an enhanced performance, even when the performance is compared to the small taper tubes and the conventional straight tubes also. Thick top plates also produced a better response for sacrificial panels, where they acted stiffer for bending deformations, and more resistant

to the plates' contacting problem. Therefore, tapered tubes outperformed straight tubes with a higher energy absorption per unit deformed length in sacrificial panels with thick top plates. Finally, it is essential to emphasize on the drastic effect the top plate holds to panels subjected to localized impulsive load, where TPT was the leading controlling parameter from a core efficiency point of view.

CHAPTER 5. CONCLUSIONS

A numerical study using the finite element code Abaqus/Explicit was conducted to test the effect of the geometrical configurations of sacrificial sandwich panels against near-field impulsive load. The panels' cores were composed of axially oriented, octagonal cross-sectioned, straight and tapered tubes. From the reviewed literature, octagonal tubes were shown to offer higher energy absorption capacity than conventional geometrical cross-sections. Furthermore, tapered tubes performed more stable under oblique loadings as compared to conventional straight tubes. The influence of the tube taper angle, tube aspect ratio, tube and top-plate thickness, the width-to-length ratio of the cross-section on the tested panels were all investigated. The force- and energy absorption-displacement characteristics, deformation modes, and a number of sacrificial panel assessment parameters composed of the peak force (PF), stroke efficiency (ε_{stroke}), energy absorption (EA) and core efficiency (ε_{core}) were analyzed. Based on the analyzed geometrical parameters, the following conclusions were made:

- By analyzing the force-displacement characteristics, tapered tubes were found to utilize higher stokes in a more stable deformation behavior. Moreover, tubes of a 5° taper (i.e., small taper) performed unfavorably exhibiting increased peak force and lower energy absorption.
- Straight tubes achieved higher EA for their top half portion (Before a mid-length of 35 mm), however, tapered tubes absorbed higher energy for their bottom portion, giving tapered tubes a slightly higher EA when employed in thick plates panels, and lower EA in thin plates' panels.
- There were four deformations modes exhibited by the tubes, and they were mainly influenced by the top-plate and tube thickness.

- With all assessment parameters taken into consideration, tubes with a 5° taper (i.e., small taper) performed unfavorably under high strain-rate oblique loading.
- Panels of top-plate thickness of 4 mm and tube thickness of 0.6 mm experienced the highest $\varepsilon_{\text{stroke}}$ with an average of 0.68, while, panels of 4 mm plate thickness and 1.2 mm tube thickness experience the lowest $\varepsilon_{\text{stroke}}$ with an average of 0.23.
- An increase of $\varepsilon_{\text{stroke}}$ with aspect ratio was found to be higher in panels with thick plates than thinner ones, with an average of 0.06 and 0.02, respectively.
- Cross-sectional ratio had minor-to-no influence on the assessment parameters, except on EA with no general trend.
- Panels with a thin top-plate (2 mm) and thick tubes (1.2 mm) resulted in the highest EA among all other panel configurations with an average of 1.79 kJ, but, it stimulated top and back plate contact, which increased the peak pressure on the non-sacrificial structures by many folds.
- A percentage increase of 73.5% in ε_{core} was observed in thick plated panels as compared to thin-plated ones, concluding with TPT being the leading parameter with respect to core efficiency.
- In designing an actual sacrificial cladding structure, localized loads cannot be ignored, since a slight divergence from a uniform load assumption might result in a completely different result of the core.

CHAPTER 6. RECOMMNEDATIONS FOR FUTURE WORK

Knowledge was added to the behavior of sacrificial panels against air blast loading from this thesis, but, additional investigations are needed to further extend the knowledge and approach for a more complete picture of the understanding in this field. Therefore, the following recommendations are proposed:

- The top plate played a significant role on the behavior exerted by the panel, so forth, the bending stiffness or the thickness were found of extreme importance. Moreover, the biggest values possible of these aforementioned parameters would assure avoiding the significant blast load localizations, which causes the oblique load. One possible solution is to account for a different material for the top plate; composite plates played an important role in this filed.
- Due to time and cost constraints, limited geometric parameters were investigated for the core tubes. Thus, the inclusion of a wider range will give a clearer picture of the behavior of axially loaded core thin-walled tubes against shock loading. Also, providing materials other than mild steel to investigate their effect on the performance.
- Due to the restrictions of conducting research utilizing blast loads, experimentations on loading structures was avoided. Therefore, carrying more experiments would be of a great benefit to the field of blast loaded structures, as it would act as a calibration basis for future analytical and numerical studies.
- Employing a multi-objective optimization study leads to the geometrical parameters that investigates the optimum performance of the panel, depending on the requested response characteristics.

- Rather than considering monolithic plates, a great deal of research should be carried on Functionally graded plates. These plates consider either different types of metals across the thickness of the plate, or, metal-fiber, metal-ceramic, or fiber-ceramic combinations. With all aforementioned material configurations possessing the potential protection measures favored in the field of impulsive/ballast loading.

REFERENCES

[1] Micallef K. The dynamic response of blast-loaded monolithic and composite plated structures A thesis submitted for the degree of Doctor of Philosophy (Ph . D .). n.d.

[2] Smith PD. Blast walls for structural protection against high explosive threats: A review. Int J Prot Struct 2010;1:67–84. doi:10.1260/2041-4196.1.1.67.

[3] Zhu F, Lu G. A review of blast and impact of metallic and sandwich structures. Electron J Struct Eng 2007;8:92–101.

[4] Louca LA, Boh JW, Choo YS. Design and analysis of stainless steel profiled blast barriers. J Constr Steel Res 2004;60:1699–723. doi:10.1016/j.jcsr.2004.04.005.

[5] Zhao H, Yu H, Yuan Y, Zhu H. Blast mitigation effect of the foamed cement-base sacrificial cladding for tunnel structures. Constr Build Mater 2015;94:710–8. doi:10.1016/j.conbuildmat.2015.07.076.

[6] Erdik A, Kilic SA, Kilic N, Bedir S. Erratum to: Numerical simulation of armored vehicles subjected to undercarriage landmine blasts. Shock Waves 2016;26:531. doi:10.1007/s00193-016-0678-4.

[7] Arora H, Del Linz P, Dear JP. Damage and deformation in composite sandwich panels exposed to multiple and single explosive blasts. Int J Impact Eng 2017;104:95–106. doi:10.1016/j.ijimpeng.2017.01.017.

[8] Jones N. Structural impact. Cambridge university press; 2011.

[9] McCallef K. The dynamic response of blast-loaded monolithic and composite plated structures. 2013. doi:10.1128/IAI.68.12.6602-6610.2000.

[10] Xiang XM, Lu G, Ma GW, Li XY, Shu DW. Blast response of sandwich beams with thin-walled tubes as core. Eng Struct 2016;127:40–8.

doi:10.1016/j.engstruct.2016.08.034.

[11] Yuen SCK, Cunliffe G, du Plessis MC. Blast response of cladding sandwich panels with tubular cores. Int J Impact Eng 2017;110:266–78. doi:10.1016/j.ijimpeng.2017.04.016.

[12] Micallef K, Fallah AS, Curtis PT, Louca LA. A study of early-time response in dynamically loaded visco-elastic composites. Compos Struct 2012;94:1366–78. doi:10.1016/j.compstruct.2011.11.033.

[13] Micallef K, Fallah AS, Curtis PT, Louca LA. A homogenised continuum constitutive model for visco-plastic deformation of uni-directional composites. Compos Struct 2013;99:404–18. doi:10.1016/j.compstruct.2012.12.006.

[14] Micallef K, Fallah AS, Pope DJ, Louca LA. The dynamic performance of simply-supported rigid-plastic circular steel plates subjected to localised blast loading. Int J Mech Sci 2012;65:177–91. doi:10.1016/j.ijmecsci.2012.10.001.

[15] Micallef K, Fallah AS, Pope DJ, Louca LA. Dynamic performance of simply supported rigid plastic circular thick steel plates subjected to localized blast loading. J Eng Mech 2013;140:159–71. doi:10.1061/(ASCE)EM.1943-7889.0000645.

[16] Goel MD. Deformation, energy absorption and crushing behavior of single-, double-and multi-wall foam filled square and circular tubes. Thin-Walled Struct 2015;90:1–11. doi:10.1016/j.tws.2015.01.004.

[17] Djamaluddin F, Abdullah S, Ariffin AK, Nopiah ZM. Optimization of foam-filled double circular tubes under axial and oblique impact loading conditions. Thin-Walled Struct 2015;87:1–11. doi:10.1016/j.tws.2014.10.015.

[18] Yin H, Wen G, Wu X, Qing Q, Hou S. Crashworthiness design of functionally graded foam-filled multi-cell thin-walled structures. Thin-Walled Struct

2014;85:142–55. doi:10.1016/j.tws.2014.08.019.

[19] Li G, Zhang Z, Sun G, Xu F, Huang X. Crushing analysis and multiobjective optimization for functionally graded foam-filled tubes under multiple load cases. Int J Mech Sci 2014;89:439–52. doi:10.1016/j.ijmecsci.2014.10.001.

[20] Reid SR. Plastic deformation mechanisms in axially compressed metal tubes used as impact energy absorbers. Int J Mech Sci 1993;35:1035–52.

[21] Mamalis AG, Robinson M, Manolakos DE, Demosthenous GA, Ioannidis MB, Carruthers J. Crashworthy capability of composite material structures. Compos Struct 1997;37:109–34.

[22] Alghamdi AAA. Collapsible impact energy absorbers: an overview. Thin-Walled Struct 2001;39:189–213.

[23] Li F, Sun G, Huang X, Rong J, Li Q. Multiobjective robust optimization for crashworthiness design of foam filled thin-walled structures with random and interval uncertainties. Eng Struct 2015;88:111–24. doi:10.1016/j.engstruct.2015.01.023.

[24] Gao Q, Wang L, Wang Y, Wang C. Crushing analysis and multiobjective crashworthiness optimization of foam-filled ellipse tubes under oblique impact loading. Thin-Walled Struct 2016;100:105–12. doi:10.1016/j.tws.2015.11.020.

[25] Xiao Z, Fang J, Sun G, Li Q. Crashworthiness design for functionally graded foam-filled bumper beam. Adv Eng Softw 2015;85:81–95. doi:10.1016/j.advengsoft.2015.03.005.

[26] Mohammadiha O, Ghariblu H. Crush behavior optimization of multi-tubes filled by functionally graded foam. Thin-Walled Struct 2016;98:627–39. doi:10.1016/j.tws.2015.10.025.

[27] Baroutaji A, Sajjia M, Olabi A-G. On the crashworthiness performance of thin-

walled energy absorbers: recent advances and future developments. Thin-Walled Struct 2017;118:137–63. doi:10.1016/j.tws.2017.05.018.

[28] Xia Z, Wang X, Fan H, Li Y, Jin F. Blast resistance of metallic tube-core sandwich panels. Int J Impact Eng 2016;97:10–28. doi:10.1016/j.ijimpeng.2016.06.001.

[29] Zhang P, Cheng Y, Liu J, Li Y, Zhang C, Hou H, et al. Experimental study on the dynamic response of foam-filled corrugated core sandwich panels subjected to air blast loading. Compos Part B Eng 2016;105:67–81. doi:10.1016/j.compositesb.2016.08.038.

[30] Qi C, Yang S, Dong F. Crushing analysis and multiobjective crashworthiness optimization of tapered square tubes under oblique impact loading. Thin-Walled Struct 2012;59:103–19. doi:10.1016/j.tws.2012.05.008.

[31] Yuen SCK, Nurick GN. The Energy-Absorbing Characteristics of Tubular Structures With Geometric and Material Modifications: An Overview. Appl Mech Rev 2008;61:020802. doi:10.1115/1.2885138.

[32] Yang K, Xu S, Shen J, Zhou S, Xie YM. Energy absorption of thin-walled tubes with pre-folded origami patterns: numerical simulation and experimental verification. Thin-Walled Struct 2016;103:33–44. doi:10.1016/j.tws.2016.02.007.

[33] Alkhatib SE, Tarlochan F, Eyvazian A. Collapse behavior of thin-walled corrugated tapered tubes. Eng Struct 2017;150:674–92. doi:10.1016/j.engstruct.2017.07.081.

[34] Theobald MD, Nurick GN. Numerical investigation of the response of sandwich-type panels using thin-walled tubes subject to blast loads. Int J Impact Eng 2007;34:134–56. doi:10.1016/j.ijimpeng.2006.04.003.

[35] Reid SR, Reddy TY. Static and dynamic crushing of tapered sheet metal tubes of rectangular cross-section. Int J Mech Sci 1986;28:623–37. doi:10.1016/0020-7403(86)90077-9.

[36] Nagel GM, Thambiratnam DP. A numerical study on the impact response and energy absorption of tapered thin-walled tubes. Int J Mech Sci 2004;46:201–16. doi:10.1016/j.ijmecsci.2004.03.006.

[37] Nagel GM, Thambiratnam DP. Dynamic simulation and energy absorption of tapered tubes under impact loading. Int J Crashworthiness 2004;9:389–99. doi:10.1533/ijcr.2004.0298.

[38] Nagel GM, Thambiratnam DP. Computer simulation and energy absorption of tapered thin-walled rectangular tubes. Thin-Walled Struct 2005;43:1225–42. doi:10.1016/j.tws.2005.03.008.

[39] Nagel GM, Thambiratnam DP. Dynamic simulation and energy absorption of tapered thin-walled tubes under oblique impact loading. Int J Impact Eng 2006;32:1595–620. doi:10.1016/j.ijimpeng.2005.01.002.

[40] Ahmad Z, Thambiratnam DP. Crushing response of foam-filled conical tubes under quasi-static axial loading. Mater Des 2009;30:2393–403. doi:10.1016/j.matdes.2008.10.017.

[41] Ahmad Z, Thambiratnam DP. Dynamic computer simulation and energy absorption of foam-filled conical tubes under axial impact loading. Comput Struct 2009;87:186–97. doi:10.1016/j.compstruc.2008.10.003.

[42] Ahmad Z, Thambiratnam DP. Application of foam-filled conical tubes in enhancing the crashworthiness performance of vehicle protective structures. Int J Crashworthiness 2009;14:349–63. doi:10.1080/13588260902775041.

[43] Ahmad Z, Thambiratnam DP, Tan ACC. Dynamic energy absorption

characteristics of foam-filled conical tubes under oblique impact loading. Int J Impact Eng 2010;37:475–88. doi:10.1016/j.ijimpeng.2009.11.010.

[44] Guler MA, Cerit ME, Bayram B, Gerçeker B, Karakaya E. The effect of geometrical parameters on the energy absorption characteristics of thin-walled structures under axial impact loading. Int J Crashworthiness 2010;15:377–90. doi:10.1080/13588260903488750.

[45] Acar E, Guler MA, Gerçeker B, Cerit ME, Bayram B. Multi-objective crashworthiness optimization of tapered thin-walled tubes with axisymmetric indentations. Thin-Walled Struct 2011;49:94–105. doi:10.1016/j.tws.2010.08.010.

[46] Taştan A, Acar E, Güler MA, Kılınçkaya Ü. Optimum crashworthiness design of tapered thin-walled tubes with lateral circular cutouts. Thin-Walled Struct 2016;107:543–53. doi:10.1016/j.tws.2016.07.018.

[47] Alkhatib SE, Tarlochan F, Hashem A, Sassi S. Collapse behavior of thin-walled corrugated tapered tubes under oblique impact. Thin-Walled Struct 2018;122:510–28. doi:10.1016/j.tws.2017.10.044.

[48] Hetherington J, Smith P. Blast and ballistic loading of structures. CRC Press; 2014.

[49] Bulson PS. Explosive loading of engineering structures. CRC Press; 2002.

[50] Karlos V, Solomon G. Calculation of blast loads for application to structural components. 2013. doi:10.2788/61866.

[51] Baker WE. Explosions in air. University of Texas press; 1973.

[52] Hopkinson B. Bitish ordnance board minutes 13565. Kew, UK, 11: The National Archives; 1915.

[53] Cranz C. Lehrbuch der ballistik (Vol. 2). Рипол Классик; 1917.

[54] Sachs RG. The dependence of blast on ambient pressure and temperature (No. BRL-466). ARMY BALLISTIC RESEARCH LAB ABERDEEN PROVING GROUND MD; 1944.

[55] Hyde DW. CONWEP-application of TM5-855-1. US Army Eng Waterw Exp Station Vicksburg, Mass 1992.

[56] Randers-Pehrson G, Bannister KA. Airblast Loading Model for DYNA2D and DYNA3D (No. ARL-TR-1310). ARMY Res LAB ABERDEEN PROVING Gr MD 1997.

[57] Kingery CN, Bulmash G. Airblast parameters from TNT spherical air burst and hemispherical surface burst. US Army Armament Dev Center, Ballist Res Lab 1984.

[58] Langdon GS, Yuen SCK, Nurick GN. Experimental and numerical studies on the response of quadrangular stiffened plates. Part II: localised blast loading. Int J Impact Eng 2005;31:85–111. doi:10.1016/j.ijimpeng.2003.09.050.

[59] Karagiozova D, Langdon GS, Nurick GN, Yuen SCK. Simulation of the response of fibre–metal laminates to localised blast loading. Int J Impact Eng 2010;37:766–82. doi:10.1016/j.ijimpeng.2009.04.001.

[60] Jacob N, Nurick GN, Langdon GS. The effect of stand-off distance on the failure of fully clamped circular mild steel plates subjected to blast loads. Eng Struct 2007;29:2723–36. doi:10.1016/j.engstruct.2007.01.021.

[61] Theobald MD, Nurick GN. Experimental and numerical analysis of tube-core claddings under blast loads. Int J Impact Eng 2010;37:333–48. doi:10.1016/j.ijimpeng.2009.10.003.

[62] Van Paepegem W, Palanivelu S, Degrieck J, Vantomme J, Reymen B, Kakogiannis D, et al. Blast performance of a sacrificial cladding with composite

tubes for protection of civil engineering structures. Compos Part B Eng 2014;65:131–46. doi:10.1016/j.compositesb.2014.02.004.

[63] Lu G, Yu TX. Energy absorption of structures and materials. Elsevier; 2003.

[64] Calladine CR, English RW. Strain-rate and inertia effects in the collapse of two types of energy-absorbing structure. Int J Mech Sci 1984;26:689–701. doi:10.1016/0020-7403(84)90021-3.

[65] Karagiozova D, Alves M, Jones N. Inertia effects in axisymmetrically deformed cylindrical shells under axial impact. Int J Impact Eng 2000;24:1083–115. doi:10.1016/S0734-743X(00)00028-2.

[66] Jones N. Several phenomena in structural impact and structural crashworthiness. Eur J Mech 2003;22:693–707. doi:10.1016/S0997-7538(03)00077-9.

[67] Marsh KJ, Campbell JD. The effect of strain rate on the post-yield flow of mild steel. J Mech Phys Solids 1963;11:49–63. doi:http://dx.doi.org/10.1016/0022-5096(63)90007-3.

[68] Maiden CJ, Green SJ. Compressive strain-rate tests on six selected materials at strain rates from 10−3 to 104 in/in/sec. J Appl Mech 1966;33:496–504. doi:10.1115/1.3625114.

[69] Hauser FE. Techniques for measuring stress-strain relations at high strain rates. Exp Mech 1966;6:395–402.

[70] Cowper GR, Symonds PS. Strain-hardening and strain-rate effects in the impact loading of cantilever beams. Brown Univ Provid Ri 1957:1–46.

[71] Abramowicz W, Jones N. Dynamic axial crushing of circular tubes. Int J Impact Eng 1984;2:263–81.

[72] Tarlochan F, Samer F, Hamouda AMS, Ramesh S, Khalid K. Design of thin wall structures for energy absorption applications: enhancement ofcrashworthiness

due to axial and oblique impact forces. Thin-Walled Struct 2013;71:7–17. doi:10.1016/j.tws.2013.04.003.

[73] Johnson GR, Cook WH. A constitutive model and data for materials subjected to large strains, high strain rates, and high temperatures. 7th Int. Symp. Ballist., The Hague, The Netherlands: 1983, p. 541–547.

[74] Karagiozova D, Nurick GN, Chung Kim Yuen S. Energy absorption of aluminium alloy circular and square tubes under an axial explosive load. Thin-Walled Struct 2005;43:956–82. doi:10.1016/j.tws.2004.11.002.

[75] Liang R, Khan AS. A critical review of experimental results and constitutive models for BCC and FCC metals over a wide range of strain rates and temperatures. Int J Plast 1999;15:963–80.

[76] Palanivelu S, Van Paepegem W, Degrieck J, Reymen B, Ndambi J-M, Vantomme J, et al. Close-range blast loading on empty recyclable metal beverage cans for use in sacrificial cladding structure. Eng Struct 2011;33:1966–87. doi:10.1016/j.engstruct.2011.02.034.

[77] Jacob N, Yuen SCK, Nurick GN, Bonorchis D, Desai SA, Tait D. Scaling aspects of quadrangular plates subjected to localised blast loads—experiments and predictions. Int J Impact Eng 2004;30:1179–208. doi:10.1016/j.ijimpeng.2004.03.012.

[78] Yuen SCK, Nurick GN, Langdon GS, Iyer Y. Deformation of thin plates subjected to impulsive load: Part III–an update 25 years on. Int J Impact Eng 2017;107:108–17. doi:10.1016/j.ijimpeng.2016.06.010.

[79] Nurick GN, Martin JB. Deformation of thin plates subjected to impulsive loading—a review: Part i: Theoretical considerations. Int J Impact Eng 1989;8:159–70. doi:10.1016/0734-743X(89)90014-6.

[80] Li QM, Jones N. On dimensionless numbers for dynamic plastic response of structural members. Arch Appl Mech 2000;70:245–54. doi:10.1007/s004199900072.

[81] Yuen SCK, Nurick GN. The Use of Tubular Structures as Cores for Sandwich Panels Subjected to Dynamic and Blast Loading: A Current “State of the Art.” In: Shukla A, Rajapakse YDS, Hynes ME, editors. Blast Mitig., New York, NY: Springer; 2014, p. 229–48. doi:10.1007/978-1-4614-7267-4.

[82] Shim VP, Stronge WJ. Lateral crushing of thin-walled tubes between cylindrical indenters. Int J Mech Sci 1986;28:683–707. doi:10.1016/0020-7403(86)90013-5.

[83] Jin X, Wang Z, Ning J, Xiao G, Liu E, Shu X. Dynamic response of sandwich structures with graded auxetic honeycomb cores under blast loading. Compos Part B Eng 2016;106:206–17. doi:10.1016/j.compositesb.2016.09.037.

[84] Abramowicz W, Jones N. Dynamic progressive buckling of circular and square tubes. Int J Impact Eng 1986;4:243–70.

[85] Guillow SR, Lu G, Grzebieta RH. Quasi-static axial compression of thin-walled circular aluminium tubes. Int J Mech Sci 2001;43:2103–23. doi:10.1016/S0020-7403(01)00031-5.

[86] Singace AA. Axial crushing analysis of tubes deforming in the multi-lobe mode. Int J Mech Sci 1999;41:865–90. doi:10.1016/S0020-7403(98)00052-6.

[87] Tang Z, Liu S, Zhang Z. Analysis of energy absorption characteristics of cylindrical multi-cell columns. Thin-Walled Struct 2013;62:75–84. doi:10.1016/j.tws.2012.05.019.

[88] Rossi A, Fawaz Z, Behdinan K. Numerical simulation of the axial collapse of thin-walled polygonal section tubes. Thin-Walled Struct 2005;43:1646–61.

doi:10.1016/j.tws.2005.03.001.

[89] Witteman WJ. Improved Vehicle Crashworthiness Design by Control of the Energy Absorption for Different Collision Situations. Eindhoven: Technische Universiteit Eindhoven, 1999. doi:10.6100/IR518429.

[90] Abramowicz W, Wierzbicki T. Axial crushing of multicorner sheet metal columns. J Appl Mech 1989;56:113–20. doi:10.1115/1.3176030.

[91] Mamalis AG, Manolakos DE, Baldoukas AK, Viegelahn GL. Energy dissipation and associated failure modes when axially loading polygonal thin-walled cylinders. Thin-Walled Struct 1991;12:17–34. doi:10.1016/0263-8231(91)90024-D.

[92] Mamalis AG, Manolakos DE, Ioannidis MB, Kostazos PK, Dimitriou C. Finite element simulation of the axial collapse of metallic thin-walled tubes with octagonal cross-section. Thin-Walled Struct 2003;41:891–900. doi:10.1016/S0263-8231(03)00046-6.

[93] Tang Z, Liu S, Zhang Z. Energy absorption properties of non-convex multi-corner thin-walled columns. Thin-Walled Struct 2012;51:112–20. doi:10.1016/j.tws.2011.10.005.

[94] Zhang X, Huh H. Crushing analysis of polygonal columns and angle elements. Int J Impact Eng 2010;37:441–51. doi:10.1016/j.ijimpeng.2009.06.009.

[95] Abbasi M, Reddy S, Ghafari-Nazari A, Fard M. Multiobjective crashworthiness optimization of multi-cornered thin-walled sheet metal members. Thin-Walled Struct 2015;89:31–41. doi:10.1016/j.tws.2014.12.009.

[96] Fan Z, Lu G, Liu K. Quasi-static axial compression of thin-walled tubes with different cross-sectional shapes. Eng Struct 2013;55:80–9. doi:10.1016/j.engstruct.2011.09.020.

[97] Thornton PH, Magee CL. The interplay of geometric and materials variables in energy absorption. J Eng Mater Technol 1977;99:114–20. doi:10.1115/1.3443419.

[98] Gupta NK, Gupta SK. Effect of annealing, size and cut-outs on axial collapse behaviour of circular tubes. Int J Mech Sci 1993;35:597–613. doi:10.1016/0020-7403(93)90004-E.

[99] Abramowicz W, Jones N. Transition from initial global bending to progressive buckling of tubes loaded statically and dynamically. Int J Impact Eng 1997;19:415–37. doi:10.1016/S0734-743X(96)00052-8.

[100] Karagiozova D, Alves M. Transition from progressive buckling to global bending of circular shells under axial impact—Part I: Experimental and numerical observations. Int J Solids Struct 2004;41:1565–80. doi:10.1016/j.ijsolstr.2003.10.005.

[101] Reid SR, Reddy TY. Axial crushing of foam-filled tapered sheet metal tubes. Int J Mech Sci 1986;28:643–56.

[102] Shrot A, Bäker M. Determination of Johnson–Cook parameters from machining simulations. Comput Mater Sci 2012;52:298–304. doi:10.1063/1.3589487.

[103] Mamalis AG, Johnson W. The quasi-static crumpling of thin-walled circular cylinders and frusta under axial compression. Int J Mech Sci 1983;25:713–32. doi:10.1002/andp.18290920508.

[104] Nagel G. Impact and Energy Absorption of Straight and Tapered Rectangular Tubes 2005.

[105] Remennikov AM, Uy B. Explosive testing and modelling of square tubular steel columns for near-field detonations. J Constr Steel Res 2014;101:290–303. doi:10.1016/j.jcsr.2014.05.027.

[106] Jin X, Wang Z, Ning J, Xiao G, Liu E, Shu X. Dynamic response of sandwich structures with graded auxetic honeycomb cores under blast loading. Compos Part B Eng 2016;106:206–17. doi:10.1016/j.compositesb.2016.09.037.

[107] Zhu F, Zhao L, Lu G, Wang Z. Deformation and failure of blast-loaded metallic sandwich panels—experimental investigations. Int J Impact Eng 2008;35:937–51. doi:10.1016/j.ijimpeng.2007.11.003.

[108] Zhu F, Zhao L, Lu G, Gad E. A numerical simulation of the blast impact of square metallic sandwich panels. Int J Impact Eng 2009;36:687–99. doi:10.1016/j.ijimpeng.2008.12.004.

[109] Theobald MD, Nurick GN. Experimental and numerical analysis of tube-core claddings under blast loads. Int J Impact Eng 2010;37:333–48. doi:10.1016/j.ijimpeng.2009.10.003.

[110] Manual ABAQUS. Getting Started with Abaqus: Interactive Edition 2008;version 6.

[111] Wu S, Li G, Sun G, Wu X, Li Q. Crashworthiness analysis and optimization of sinusoidal corrugation tube. Thin-Walled Struct 2016;105:121–34. doi:10.1016/j.tws.2016.03.029.

APPENDIX

Table 14. Summary of the Panels' Responses

TPT (mm)	CSR	t (mm)	θ (°)	R	L (mm)	PF (kN)	P_{mean} (kN)	ε_{stroke}	EA (kJ)	ε_{core}	Plates contact
4	1	0.6	0	3	75	79.12	39.76	0.53	1.59	0.68	no
4	1	0.6	5	3	75	86.93	35.58	0.60	1.59	0.68	no
4	1	0.6	10	3	75	85.65	34.36	0.63	1.62	0.69	no
4	1	0.6	0	4	75	57.24	33.08	0.65	1.61	0.68	no
4	1	0.6	5	4	75	65.39	31.87	0.68	1.62	0.68	no
4	1	0.6	10	4	75	53.94	30.43	0.71	1.62	0.68	yes
4	1	0.6	0	5	75	46.04	29.62	0.71	1.58	0.67	yes
4	1	0.6	5	5	75	54.48	28.21	0.71	1.50	0.63	yes
4	1	1.2	0	3	75	158.18	95.06	0.16	1.13	0.49	no
4	1	1.2	5	3	75	179.96	88.35	0.17	1.15	0.49	no
4	1	1.2	10	3	75	155.43	76.19	0.21	1.18	0.50	no
4	1	1.2	0	4	75	115.46	77.18	0.20	1.17	0.50	no
4	1	1.2	5	4	75	131.39	73.93	0.22	1.21	0.51	no
4	1	1.2	10	4	75	110.40	62.99	0.27	1.28	0.54	no
4	1	1.2	0	5	75	92.63	66.31	0.25	1.24	0.53	no
4	1	1.2	5	5	75	107.35	63.06	0.27	1.29	0.55	no
2	1	0.6	0	3	75	80.42	44.55	0.49	1.63	0.35	yes
2	1	0.6	5	3	75	89.42	38.75	0.49	1.42	0.30	yes
2	1	0.6	10	3	75	86.00	35.23	0.49	1.30	0.28	yes
2	1	0.6	0	4	75	57.98	38.83	0.50	1.44	0.31	yes

TPT (mm)	CSR	t (mm)	θ (°)	R	L (mm)	PF (kN)	P_{mean} (kN)	ε_{stroke}	EA (kJ)	ε_{core}	Plates contact
2	1	0.6	5	4	75	65.00	33.89	0.50	1.26	0.27	yes
2	1	0.6	10	4	75	56.52	30.12	0.51	1.16	0.24	yes
2	1	0.6	0	5	75	46.53	33.21	0.50	1.25	0.26	yes
2	1	0.6	5	5	75	54.39	29.62	0.52	1.15	0.24	yes
2	1	1.2	0	3	75	165.79	72.63	0.36	1.97	0.43	yes
2	1	1.2	5	3	75	185.85	69.35	0.36	1.87	0.40	yes
2	1	1.2	10	3	75	172.99	63.77	0.36	1.73	0.37	yes
2	1	1.2	0	4	75	120.22	66.12	0.37	1.85	0.40	yes
2	1	1.2	5	4	75	134.72	60.55	0.37	1.68	0.36	yes
2	1	1.2	10	4	75	105.10	56.82	0.47	2.02	0.43	yes
2	1	1.2	0	5	75	93.33	58.33	0.39	1.69	0.36	yes
2	1	1.2	5	5	75	106.60	54.12	0.39	1.58	0.34	yes
4	2	0.6	0	3	75	79.60	32.99	0.64	1.59	0.68	no
4	2	0.6	5	3	75	84.64	32.86	0.65	1.59	0.68	no
4	2	0.6	10	3	75	83.28	34.64	0.70	1.82	0.77	no
4	2	0.6	0	4	75	57.72	26.49	0.76	1.50	0.64	yes
4	2	0.6	5	4	75	65.36	27.63	0.71	1.47	0.62	yes
4	2	0.6	10	4	75	54.21	27.31	0.72	1.48	0.62	yes
4	2	0.6	0	5	75	45.45	25.55	0.73	1.40	0.59	yes
4	2	0.6	5	5	75	54.01	22.55	0.79	1.34	0.56	yes
4	2	1.2	0	3	75	158.32	96.09	0.16	1.13	0.49	no
4	2	1.2	5	3	75	169.91	90.91	0.17	1.13	0.48	no
4	2	1.2	10	3	75	155.75	74.26	0.24	1.35	0.57	no

TPT (mm)	CSR	t (mm)	θ (°)	R	L (mm)	PF (kN)	P_{mean} (kN)	ε_{stroke}	EA (kJ)	ε_{core}	Plates contact
4	2	1.2	0	4	75	115.35	81.56	0.19	1.16	0.50	no
4	2	1.2	5	4	75	132.19	78.01	0.20	1.15	0.49	no
4	2	1.2	10	4	75	110.32	53.52	0.35	1.40	0.59	no
4	2	1.2	0	5	75	91.65	70.88	0.23	1.22	0.52	no
4	2	1.2	5	5	75	102.94	59.87	0.32	1.45	0.61	no
2	2	0.6	0	3	75	80.61	38.93	0.48	1.40	0.59	yes
2	2	0.6	5	3	75	89.75	40.33	0.47	1.44	0.31	yes
2	2	0.6	10	3	75	86.44	33.98	0.53	1.35	0.29	yes
2	2	0.6	0	4	75	58.08	32.90	0.49	1.20	0.26	yes
2	2	0.6	5	4	75	65.65	33.73	0.49	1.23	0.26	yes
2	2	0.6	10	4	75	55.87	27.75	0.51	1.07	0.23	yes
2	2	0.6	0	5	75	45.05	28.89	0.54	1.17	0.25	yes
2	2	0.6	5	5	75	53.86	25.28	0.51	0.97	0.21	yes
2	2	1.2	0	3	75	164.30	72.20	0.35	1.89	0.41	yes
2	2	1.2	5	3	75	185.80	72.66	0.34	1.87	0.40	yes
2	2	1.2	10	3	75	173.77	64.88	0.45	2.18	0.47	yes
2	2	1.2	0	4	75	120.53	69.30	0.36	1.88	0.40	yes
2	2	1.2	5	4	75	136.50	31.96	0.35	0.84	0.18	yes
2	2	1.2	10	4	75	107.68	56.17	0.37	1.57	0.33	yes
2	2	1.2	0	5	75	95.32	64.20	0.49	2.34	0.50	yes
2	2	1.2	5	5	75	104.50	58.97	0.37	1.64	0.35	yes